

Reviewed Preprint

v1 • June 11, 2026

Not revised

✉ For correspondence:

xwang@jiangnan.edu.cn

xiaoyun.liu@bjmu.edu.cn

ayan8@hku.hk

* These authors contributed equally

† Lead contact

Competing interests: No

competing interests declared

Funding: See page 53

Reviewing editor: Sloan Siegrist,
University of Massachusetts
Amherst, United States© 2026, Zhang et al. This article is
distributed under the terms of the[Creative Commons Attribution](#)[License](#), which permits unrestricted
use and redistribution provided that
the original author and source are
credited.

Identifying and targeting the Mg-Fe-PmrAB regulatory circuit reverses phosphate starvation-driven polymyxin resistance in *Enterobacteriaceae*

Guangming Zhang¹, Ziqing Deng^{1,6,*}, Jiezhong Jiang^{2,3,*}, Minji Wang^{1,7}, Xiaoyuan Wang^{4,5}✉, Xiaoyun Liu^{2,3}✉, Aixin Yan^{1,†}✉¹School of Biological Sciences, Faculty of Science, The University of Hong Kong, Hong Kong SAR, China • ²Department of Microbiology and Infectious Disease Center, NHC Key Laboratory of Medical Immunology, School of Basic Medical Sciences, Peking University Health Science Center, Beijing, China • ³Department of Infectious Diseases, Peking University Third Hospital, Beijing, China • ⁴State Key Laboratory of Food Science and Resources, Jiangnan University, Wuxi, China • ⁵School of Biotechnology, Jiangnan University, Wuxi, China • ⁶BGI Research, Beijing, China • ⁷School of Chemistry and Material Sciences, University of Shanghai for Science and Technology, Shanghai, China

eLife Assessment

This study characterizes a potentially targetable mechanism by which phosphate scarcity drives polymyxin B resistance in *Enterobacteriaceae*. The findings are **important**. While some aspects of the approach are very strong, particularly the diversity of techniques, it is recommended to include genetic controls and antibiotic resistance experiments in order to strengthen the evidence, which is currently **solid**. The clarity and presentation of the findings could also be improved.

<https://doi.org/10.7554/eLife.111143.1.sa3>

Abstract

Phosphate (Pi) scarcity, a pervasive stressor prevalent in bacterial infections and dysbiotic host environments, potently drives antimicrobial resistance (AMR) against cationic antibiotics like polymyxins across diverse bacterial taxa. While established Pi depletion-induced AMR mechanisms often involve membrane phospholipid remodelling, *Enterobacteriaceae* largely lack these pathways, leaving their Pi scarcity-driven AMR mechanism unresolved. Here, we reveal that Pi limitation robustly induces polymyxin resistance in *Enterobacteriaceae* through 4-amino-4-deoxy-L-arabinose (L-Ara4N) modification of the Gram-negative outer membrane component lipid A, reflecting a distinct adaptive strategy. This modification is driven by strong *ugd-arn* operon induction, mediated by the PmrAB two-component system. We discover that Pi depletion triggers cellular Mg²⁺ release, prompting compensatory Fe³⁺ mobilization to the cell envelope that directly activates PmrAB. Crucially, this metal-dependent signaling axis offers a directly targetable mechanism for reversing polymyxin resistance, a significant deviation from the less accessible, PhoBR-regulated phospholipid remodelling strategies in other bacteria. We demonstrate that Mg²⁺ supplementation or Fe³⁺ chelation effectively suppresses PmrAB activation and restores polymyxin susceptibility, thereby establishing a novel, metal-centric paradigm for understanding and pharmacological intervention in stress-induced AMR.

Introduction

Within the dynamic and often hostile environment of the host, nutrient scarcity presents a pervasive challenge for invading bacteria, promoting the evolution of survival strategies and shaping pathogen persistence.^{1,2} Among the macronutrients essential for bacteria, phosphorus (P) serves as a critical element for life. It is a fundamental component of key biomolecules such as nucleic acids, phospholipids, and ATP, and plays crucial roles in the essential processes of genetic inheritance, energy metabolism, membrane integrity, and signal transduction.^{3,4} The primary assimilable form of phosphorus for bacteria is the orthophosphate anion (PO_4^{3-}), commonly known as inorganic phosphate (Pi). However, Pi is typically found at very low concentrations ($<4\mu\text{M}$) in diverse environments, from oceans ($0.1\text{--}3\mu\text{M}$),^{5,6} and soil (0.0105 to $10.5\mu\text{M}$, $<1\mu\text{M}$ near plant roots),^{7,8} to critically host-associated niches including macrophages,⁹ Salmonella-containing vacuoles,¹⁰ and cystic fibrosis sputum.¹¹ This localized Pi scarcity is a direct consequence of host nutritional immunity and intense microbial competition.^{12,13} Evidence for widespread bacterial adaptation to Pi limitation is abundant, with metagenomic and metatranscriptomic studies consistently revealing robust transcriptional upregulation of high-affinity phosphate acquisition (Pho) regulon genes across various chronic infections and dysbiosis conditions.^{11,14,15} Bacteria cope with these pervasive conditions via the conserved PhoBR two-component system, which activates genes for Pi acquisition, transport, and storage when extracellular Pi falls below $4\mu\text{M}$.^{3,16,17}

Beyond direct Pi assimilation, Pi depletion triggers broader adaptive responses crucial for pathogen survival, including enhanced virulence and, critically, antimicrobial resistance (AMR).^{18–20} For example, Pi limitation upregulates virulence factors in *Vibrio cholerae*, EHEC, and *Pseudomonas aeruginosa*, and conversely, Pi supplementation can reduce infection severity.^{21–24} More importantly, Pi depletion is increasingly recognized as a potent environmental cue driving AMR across diverse bacterial taxa, particularly against cationic antibiotics like polymyxins. This is evidenced by increased vancomycin resistance in *Streptomyces coelicolor*,²⁵ and enhanced polymyxin B/E resistance in *Pseudomonas fluorescens*, *P. aeruginosa*, and *Acinetobacter baumannii* under Pi-limited conditions.^{11,26–28} Given that Pi limitation is a prevalent and dynamic stressor in host niches, understanding its role in promoting AMR is vital for developing effective counter-strategies.

Mechanistically, Pi depletion-induced AMR is often linked to the remodelling of bacterial membranes, where phosphorus-containing phospholipids are substituted with diverse non-phosphorous lipids. This strategy spares intracellular phosphate and often modifies membrane charge, which is critical for resistance to cationic antimicrobials. Examples include the accumulation of ornithine lipids (OLs) in *Vibrio cholerae*,²⁹ diacylglyceryl-N,N,N-trimethylhomoserine (DGTS) in *Rhizobium meliloti*,³⁰ and *Cryptococcus neoformans*,³¹ glycolipids in *Agrobacterium tumefaciens*,³² and extensive lipidome remodelling in *Mycobacterium tuberculosis*.³³ Specifically for polymyxin resistance, *P. aeruginosa* synthesizes neutral monoglucosyl diacylglycerol (MGDG) and glucuronic acid diacylglycerol (GADG),¹¹ while *A. baumannii* produces positively charged ornithine- and lysine-containing aminolipids (OL and LL) under Pi limitation.²⁷ These diverse lipid modifications effectively reduce the net negative charge of the bacterial membrane, decreasing polymyxin binding and improving resistance.

However, these established lipid-remodelling strategies are not universally conserved. Critically, genes for OL biosynthesis are absent in most *Enterobacteriaceae*, a family of paramount clinical importance, and MGDG/GADG synthesis is not a predominant mechanism for polymyxin resistance in this group.^{34–36} Given the widespread prevalence of Pi limitation in host environments and the escalating threat of polymyxin resistance in *Enterobacteriaceae*, a fundamental question with significant clinical implications arises: what alternative, yet unidentified, mechanisms underpin Pi depletion-induced polymyxin resistance in this critical bacterial family, especially in the absence of the established OL and MGDG/GADG pathways?

In this study, we address this critical gap by reporting that Pi limitation also induces polymyxin resistance in *Enterobacteriaceae*, but through a distinct mechanism. Using *E. coli* K-12 MG1655 as a model, we demonstrate that this process involves the upregulation of conserved Ugd and ArnBCADTEF proteins, which catalyse the addition of the positively charged 4-amino-4-deoxy-L-arabinose (L-Ara4N) to lipid A. This adaptive lipid A modification is driven by a novel Pi-Mg-Fe-PmrAB regulatory circuit: loss of membrane-stabilizing magnesium (Mg^{2+}) and compensatory iron (Fe^{3+}) mobilization to the cell membrane activate the PmrAB two-component system, leading to upregulation of the *ugd-arn* operon. Crucially, interfering with this circuit, via Mg^{2+} supplementation or iron chelation, effectively reverses resistance in representative *Enterobacteriaceae* species, but not in non-enteric species like *P. aeruginosa*. Phylogenetic analyses further reveal distinct clades for *E. coli* PmrB (EcoPmrB) and *P. aeruginosa* PmrB (PaePmrB), with PaePmrB lacking the conserved “ExxE” motif required for Fe^{3+} sensing. Our findings uncover a conserved, targetable stress-responsive circuit underlying Pi depletion-induced polymyxin resistance within *Enterobacteriaceae*, offering new avenues for managing stress-induced antibiotic resistance.

Results

Pi depletion induces polymyxin resistance in *Enterobacteriaceae*

To investigate whether Pi limitation induces antibiotic resistance in *Enterobacteriaceae*, we assessed the susceptibility of two representative species, *E. coli* MG1655 and *Salmonella enterica* serovar Typhimurium ATCC14028. Bacteria were initially cultured in standard MOPS synthetic minimal medium containing replete Pi (1.32 mM). Subsequently, cultures were transferred to either Pi-replete (Pi+, 1.32 mM) or acute Pi-depleted (Pi-, 0 mM) conditions for 3 hours, a protocol adapted from R G Groat et. al.³⁷ Following this, bacterial survival was determined via 3-hour polymyxin B killing assays (Figure S1 [↗](#)). Polymyxin B concentrations for these assays were established based on the minimum inhibitory concentrations (MICs) of strains in MOPS minimal medium (Table S1 [↗](#)) and a preliminary dose-dependent killing assay (Figure S2 [↗](#)). Results showed that Pi depletion enhanced the survival of both species against polymyxin B (Figure 1A [↗](#)). Similar Pi depletion-induced polymyxin resistance was also observed in *E. coli* O157 and four uropathogenic *E. coli* strains isolated from urinary tract infection patients in the Queen Mary Hospital, Hong Kong (Figure 1B [↗](#)). Consistent with previous reports, *P. aeruginosa* PAO1 subjected to Pi depletion also display enhanced resistance against polymyxin B (Figure 1B [↗](#)). These results suggest that Pi depletion-induced polymyxin resistance is a widespread phenomenon among Gram-negative bacteria.

Pi depletion induces 4-amino-4-deoxy-L-arabinose (L-Ara-4N) modification of lipid A in *Enterobacteriaceae*

Since these species lack the MGDG/GADG and OL pathways described in *P. aeruginosa* and *A. baumannii*, we employed *E. coli* K-12 MG1655 as a model to comprehensively investigate the regulatory mechanisms underlying this stress-induced polymyxin resistance. We performed quantitative proteomic analysis on *E. coli* MG1655 cells subjected to the identical growth and treatment conditions as for the polymyxin B challenging assay (Figure S1 [↗](#)). Among the 2990 proteins detected which cover 69% of the 4358 proteins annotated in the UniProt *E. coli* MG1655 database, abundance of 225 proteins was found to be altered following acute Pi depletion, with 142 proteins upregulated and 83 downregulated (Figure S3 [↗](#)) (Table S2 [↗](#)). In addition to proteins belonging to the Pho regulon, such as PhoB, PstB, PhoU, and PhnB (Figure 2A [↗](#)) in the COG functional group of transportation and metabolism of inorganic ions (13% of upregulated proteins) (Figure S3 [↗](#)), the most abundant functional groups among the significantly upregulated proteins include those involved in cell wall/membrane/envelope biogenesis (13%) and energy production and conversion (10%) (Figure S3 [↗](#)). Conversely, proteins involved in translation, ribosomal structure and biogenesis (33%) and amino acid transport and metabolism (17%) were significantly downregulated (Figure S3 [↗](#)).

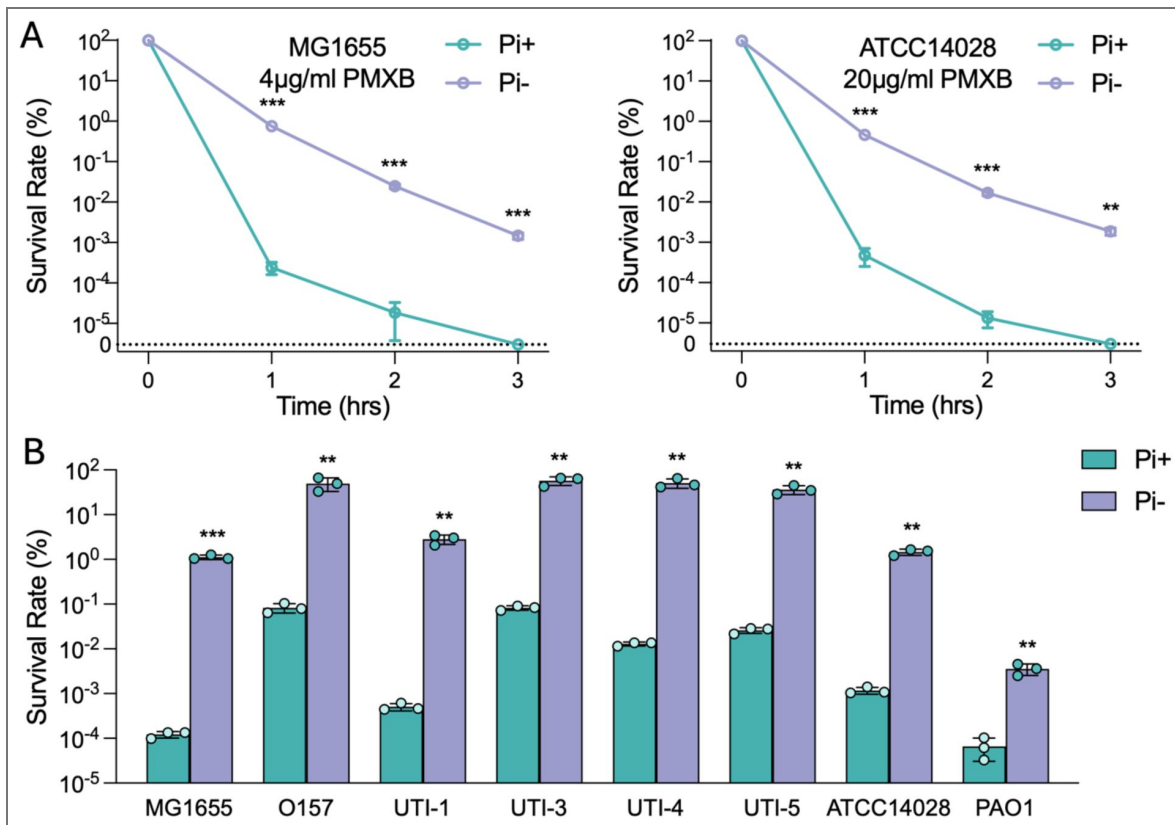


Figure 1. Pi depletion induces polymyxin resistance in diverse bacterial species.

(A) Time-kill curves of *Escherichia coli* MG1655 (left panel) and *Salmonella*. Typhimurium ATCC14028 (right panel) exposed to polymyxin B (PMXB) (4 µg/ml for *E. coli* strains, 20 µg/ml for *S. Typhimurium*) following acute Pi-starvation treatment (Pi-, 0 mM Pi) compared to the group without treatment (Pi+, 1.32 mM Pi). (B) Survival rates for various *Enterobacteriaceae* strains (*E. coli* MG1655, O157, UTI-1, UTI-3, UTI-4, UTI-5, *S. Typhimurium* ATCC14028) and *Pseudomonas aeruginosa* PAO1 exposed 1-hour to polymyxin B (4 µg/ml for *E. coli* strains, 20 µg/ml for *S. Typhimurium* and 8 µg/ml for *P. aeruginosa*). For all tested strains, phosphate depletion (Pi-, purple bars) significantly increases polymyxin B resistance compared to phosphate-replete (Pi+, teal bars) conditions. Error bars represent the standard deviation of at least three independent experiments. Statistical significance was determined using unpaired two-tailed Student's t-test. Significance levels are indicated as follows: **p* < 0.05; ***p* < 0.01; ****p* < 0.001.

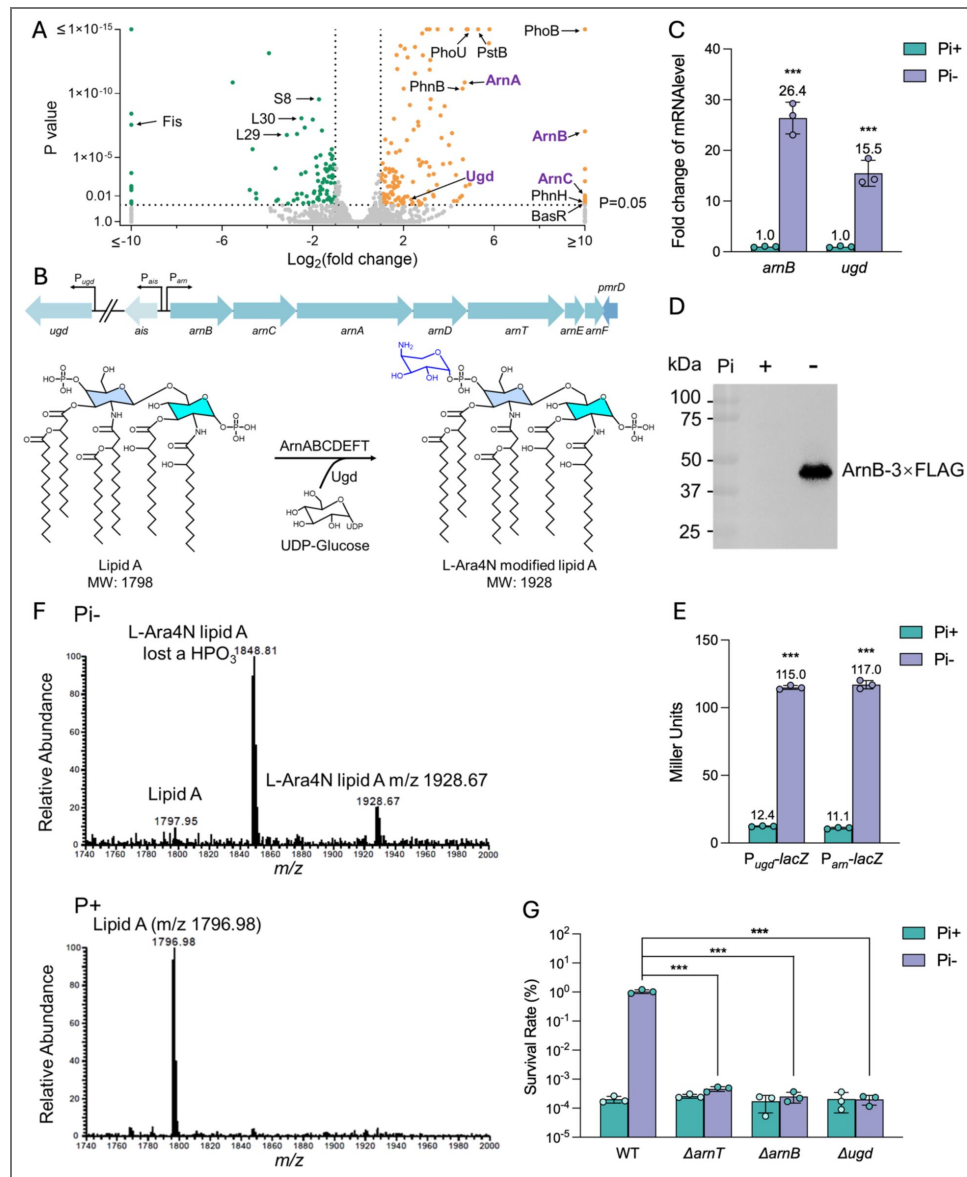


Figure 2. Pi depletion induces the expression of *ugd-arn* system to modify lipid A with L-Ara-4N, conferring stress-induced polymyxin resistance.

(A) Volcano plot depicting differentially expressed proteins in cells following acute Pi-starvation treatment (Pi-, 0 mM) compared to the group without treatment (Pi+, 1.32 mM). Red (right) and blue (left) dots represent significantly up-regulated and down-regulated proteins, respectively. The horizontal dashed line depicts a p-value cutoff (0.05), and vertical dashed lines depict 1/2 and 2-fold ratio cutoffs. Selected proteins are labeled. (B) Genetic organization of the *arn* operon and *ugd* gene in MG1655. Ugd and ArnABCDEFT catalyze the biosynthesis of 4-amino-4-deoxy-L-arabinose (L-Ara4N) and its modification of lipid A. (C) mRNA levels of *arnB* and *ugd* in cells following acute Pi-starvation treatment (Pi-, 0 mM) compared to the group without treatment (Pi+, 1.32 mM). (D) Production of ArnB-3xFLAG in cells following acute Pi-starvation treatment (Pi-, 0 mM) compared to the group without treatment (Pi+, 1.32 mM). The protein band corresponding to ArnB-3xFLAG is marked. (E) β-galactosidase activities of *P_{arn}-lacZ* and *P_{ugd}-lacZ* in MG1655 Δ *lacZ* cells following acute Pi-starvation treatment (Pi-, 0 mM) compared to the group without treatment (Pi+, 1.32 mM). (F) ESI-MS spectra of lipid A molecules extracted from *E. coli* MG1655 cells following acute Pi-starvation treatment (Pi-, 0 mM) compared to the group without treatment (Pi+, 1.32 mM). Peaks corresponding to native lipid A and L-Ara-4N modified lipid A were shown. (G) Survival rates for *E. coli* MG1655 parent and isogenic Δ *arnT*, Δ *arnB* and Δ *ugd* mutants exposed 1-hour to polymyxin B (4 μg/ml) following acute Pi-starvation treatment (Pi-, 0 mM) compared to the group without treatment (Pi+, 1.32 mM). Error bars represent the standard deviation of at least three independent experiments. Statistical significance was determined using two-tailed Student's t-test for C and E, and one-way ANOVA followed by Dunnett's multiple comparisons test for G. Significance levels are indicated as follows: **p* < 0.05; ***p* < 0.01; ****p* < 0.001.

Specifically, among the most upregulated proteins ($\log_2FC > 10$) induced by Pi depletion (Table S2 [↗](#)), two proteins encoded in the *arnBCADTEF* operon: ArnB and ArnC, were identified (Figures 2A [↗](#) and 2B [↗](#)). Additionally, two other proteins in the Arn pathway, ArnA and Ugd, were also upregulated with more than five-fold in response to Pi depletion treatment (Figures 2A [↗](#) and 2B [↗](#)). This finding is particularly intriguing, because Ugd and Arn proteins are known to catalyze the biosynthesis of 4-amino-4-deoxy-L-arabinose (L-Ara4N) and its modification of lipid A (Figure 2B [↗](#)), which confers resistance to the cationic antibiotic polymyxins due to simultaneous neutralization of a negative charge and introduction of a positive charge to lipid A.³⁸ To verify the upregulation of these proteins, we first examined the mRNA level of *ugd* and *arnB* genes by RT-qPCR and found their levels were 16- and 27-fold higher, respectively, under Pi- than under Pi+ conditions (Figure 2C [↗](#)). Next, we constructed ArnB-3×FLAG in MG1655 chromosome and observed a significant production of the ArnB protein under Pi- conditions, while its level was undetectable under Pi+ conditions (Figure 2D [↗](#)). We also constructed promoter-*lacZ* fusions and observed more than 10-fold higher promoter activities for both *ugd* and *arn* genes under Pi- conditions than Pi+ conditions (Figure 2E [↗](#)), confirming the upregulation of the Ugd-Arn system under Pi depletion.

We then extracted lipid A molecules from *E. coli* MG1655 cells cultured under identical conditions as in the proteomic analysis, and analyzed the extract using ESI-MS. Native lipid A, a hexacetylated glucosamine disaccharide with two phosphate groups at position 1 and 4' (m/z 1796.98), was detected in *E. coli* cells cultured under Pi sufficient conditions (Figure 2F [↗](#)). In constant, the predominant lipid A species in *E. coli* cells subjected to Pi depletion were found to be modified with L-Ara4N (m/z 1928.67) (Figure 2F [↗](#)). Next, we deleted *arnT*, *arnB*, and *ugd* and found that deletion of these genes abolished Pi depletion-induced polymyxin B resistance in *E. coli* (Figure 2G [↗](#)).

The induction of L-Ara4N modified lipid A, along with decrease in the unmodified form, was also observed in *E. coli* O157 (Figure S4A [↗](#)), a representative UTI strain UTI-3 (Figure S4B [↗](#)), and *S. Typhimurium* ATCC14028 (Figure S4C [↗](#)), each exhibiting varying ratios. These findings indicate that L-Ara4N modification of lipid A is widespread in *Enterobacteriaceae* and correlates with increased polymyxin B resistance. We also analyzed lipid A species in *P. aeruginosa* PAO1 and found that instead of the L-Ara4N modification, a 2-hydroxymyristate modification of lipid A, which is catalyzed by the aspartyl beta-hydroxylase LpxO, was detected in Pi-depletion treated cells (Figure S4D [↗](#)). Altogether, these results indicated that unlike the strategy observed in PAO1 where Pi stress induces resistance by replacing the negatively charged phospholipids with MGDG/GADG, in *E. coli*, resistance is mediated by lipid A modification with L-Ara4N catalyzed by Ugd and Arn proteins.

To delineate the sensitivity of the Ugd-Arn pathway to varying Pi levels, we measured the promoter activities of $P_{ugd-lacZ}$ and $P_{arn-lacZ}$ across a gradient of phosphate concentrations. We observed that the activities of both $P_{ugd-lacZ}$ and $P_{arn-lacZ}$ remained robustly activated, at levels comparable to complete Pi depletion (0 mM), even when 0.040 mM or 0.132 mM Pi was supplemented to the medium (Figure S5 [↗](#)). When Pi supplementation reached 0.4 mM, their upregulation was attenuated by 60%. These findings collectively suggest that moderate Pi limitation (below 0.4mM) is effective in sustaining the activation of *ugd-arn* genes (Figure S5 [↗](#)).

The PmrAB two component system is activated to up-regulate the *arn* operon during Pi depletion

To elucidate the regulatory mechanisms underlying *ugd-arn* upregulation during Pi limitation, we first investigated the involvement of the global phosphate regulators PhoB and PhoR. We found that deleting either PhoB or PhoR did not affect the enhanced polymyxin B resistance or the upregulation of the *arn* operon observed in Pi-depleted *E. coli* (Figures 3A [↗](#) and S6 [↗](#)). This observation suggested that other regulatory systems were primarily responsible for upregulating the *arn* gene expression under Pi depletion.

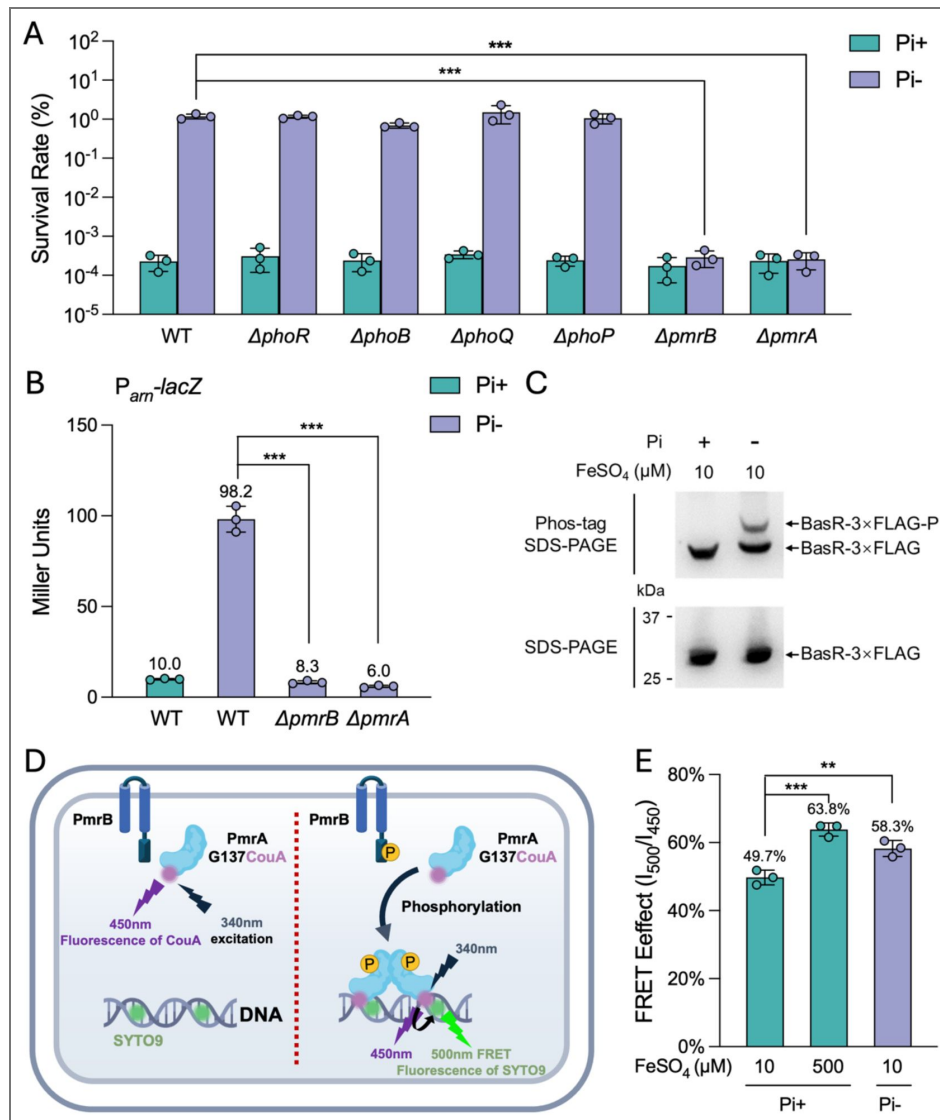


Figure 3. The PmrAB two-component system is activated during Pi depletion and is responsible for the up-regulation of *arn* genes under this condition.

(A) Survival rates for *E. coli* MG1655 parent and isogenic $\Delta pmrB$, $\Delta pmrA$, $\Delta phoB$, and $\Delta phoR$ mutants exposed 1-hour to polymyxin B (4 μg/ml) following acute Pi-starvation treatment (Pi-, 0 mM) compared to the group without treatment (Pi+, 1.32 mM). (B) β-galactosidase activities of P_{arn} -lacZ in MG1655 $\Delta lacZ$ parent and isogenic $\Delta pmrB$, $\Delta pmrA$, $\Delta phoB$, and $\Delta phoR$ mutants following acute Pi-starvation treatment (Pi-, 0 mM) compared to the group without treatment (Pi+, 1.32 mM). (C) Phosphorylation of PmrA-3xFLAG detected by Phos-Tag SDS-PAGE following immunoblotting with anti-FLAG antibody in cells following acute Pi-starvation treatment (Pi-, 0 mM) compared to the group without treatment (Pi+, 1.32 mM). Protein bands representing PmrA-3xFLAG and PmrA-3xFLAG-P are indicated. (D) Schematic diagram of the whole-cell FRET measurement of PmrA-promoter binding assay. A bright fluorescent unnatural amino acid donor CouA (red spheres) is incorporated into G137 of PmrA in DNA-binding domain. SYTO9 (green spheres) is employed to stain chromosome DNA in living *E. coli* MG1655. (E) Quantification of the FRET effect between the CouA-SYTO9 pair in *E. coli* cells following acute Pi-starvation treatment (Pi-, 0 mM Pi, 10 μM Fe) or iron excess treatment (Pi+, 1.32 mM Pi, 500 μM FeSO₄) compared to the group without treatment (Pi+, 1.32 mM Pi, 10 μM FeSO₄). Error bars represent the standard deviation of at least three independent experiments. Statistical significance was determined using one-way ANOVA followed by Dunnett's multiple comparisons test for A, B, and E. Significance levels are indicated as follows: **p* < 0.05; ***p* < 0.01; ****p* < 0.001.

The *arn* operon and *ugd* are known targets of the PmrAB two-component system (TCS) in *E. coli*.³⁹ (Note the *E. coli* homolog of this system is BasSR; we adopt the PmrAB nomenclature in this study to reflect its direct role in polymyxin resistance and its wider usage in the literature.)⁴⁰ To determine if this regulation also extended to Pi depletion, we constructed $\Delta pmrB$ and $\Delta pmrA$ mutants. Both the enhanced polymyxin B resistance and the upregulation of the *arn* operon under Pi depletion were abolished in these mutants (Figures 3A [↗](#) and 3B [↗](#)), indicating a critical role for PmrAB in *arn* regulation and polymyxin B resistance during Pi depletion. The promoter activity of *ugd* remained unaffected in $\Delta pmrB$ and $\Delta pmrA$ mutants (Figure S7 [↗](#)), suggesting a distinct regulatory input for *ugd*. Given that the PhoPQ TCS can indirectly activate the PmrAB regulon in *S. Typhimurium* via PmrD (though this indirect regulation appears absent in *E. coli*), we also examined the contribution of PhoPQ.⁴¹ Deletion of *phoP* or *phoQ* did not alter the enhanced polymyxin B resistance or *arn* operon upregulation under Pi depletion (Figures 3A [↗](#) and S6 [↗](#)). These findings suggest that the *arn* system is activated by PmrAB in response to an as-yet-unidentified secondary signal induced by Pi depletion, rather than by direct Pi depletion sensing or through the PhoPQ system.

Given the distinct regulation we observed for *ugd* promoter activity, we further investigated its response to the PhoBR system. We measured *ugd* promoter activity in $\Delta phoB$, $\Delta phoR$, $\Delta phoP$, and $\Delta phoQ$ mutants and found $P_{ugd-lacZ}$ activity decreased by approximately 30% in both $\Delta phoB$ and $\Delta phoR$ mutants, but not in $\Delta phoP$ and $\Delta phoQ$ mutants (Figure S7 [↗](#)). This indicates that *ugd* is regulated by the PhoBR system, potentially alongside other pathways, during Pi depletion.

Given the central role of the PmrAB system in mediating Pi depletion-induced polymyxin resistance, we next investigated whether *eptA*, another PmrAB-regulated gene, contributes to this phenotype. We constructed a $\Delta eptA$ mutant and assessed bacterial survival in a polymyxin B killing assay. Deletion of *eptA* had no impact on the enhanced polymyxin B resistance (Figure S8 [↗](#)), indicating that *eptA* is not required for the resistance phenotype induced by Pi depletion. This observation was further supported by ESI-MS analysis (Figure 2F [↗](#)), which did not detect phosphoethanolamine (pEtN) modification of lipid A, a hallmark of EptA activity, in Pi-depleted cells. Collectively, these results strongly suggest that the activation of the Arn system via PmrAB is the primary mechanism responsible for Pi depletion-induced polymyxin resistance.

To assess whether PmrAB activation occurs under Pi depletion, we examined the phosphorylation status of the response regulator PmrA using Phos-tag SDS-PAGE, which reliably detects phosphorylated PmrA in cells treated with known activator Fe^{3+} .⁴² Results showed that phosphorylated PmrA was detected in cells subjected to Pi depletion (Figure 3C [↗](#)), demonstrating that PmrAB TCS is indeed activated under Pi depletion condition. To further confirm this *in vivo*, we performed a FRET-based whole-cell transcription factor-promoter binding assay.⁴³ We incorporated a bright fluorescent unnatural amino acid, L-(7-hydroxycoumarin-4-yl) ethylglycine (CouA)⁴⁴ at position G137 within the DNA-binding domain of PmrA through genetic encoding, allowing it to serve as the FRET donor (Figure 3D [↗](#)).⁴³ The nucleic acid dye SYTO9 was utilized to stain promoter DNA of PmrA regulon (Figure 3D [↗](#)),⁴³ acting as the FRET acceptor. The whole-cell FRET assay revealed that, similar to the treatment with excessive $FeSO_4$ (500 μM),⁴³ a FRET signal indicative of PmrA binding to its target promoters was observed in cells subjected to Pi depletion without excessive $FeSO_4$ (Figure 3E [↗](#)). These results confirmed that Pi depletion induced activation of the PmrAB signal transduction system in *E. coli*.

Pi depletion drives Fe^{3+} elevation in *E. coli* cells to activate the PmrAB TCS

PmrAB has been previously reported to be activated by ferric ion (Fe^{3+}), zinc ions (Zn^{2+}), aluminum ions (Al^{3+}), or acidic pH.^{45,46} Since no Al^{3+} was added in the culture, and the pH remained largely unchanged (7.2-7.0) across the Pi depletion treatments (Figure S9 [↗](#)), we focused on the two metal ions and examined cellular metal profiles including iron (Fe), zinc (Zn), magnesium (Mg), copper (Cu), and calcium (Ca). ICP-MS analysis revealed a significant, greater than 5-fold increase in cellular Fe content under Pi depletion, compared to Pi-sufficient conditions

(Figure 4A [↗](#)). Conversely, cellular Mg levels decreased, while Cu, Zn, and Ca levels remained largely unchanged (Figure 4A [↗](#)). Corroborating this cellular Fe accumulation, the Fe content in the spent medium decreased after 3 hours of *E. coli* incubation under Pi depletion (Figure 4B [↗](#)), indicating active Fe mobilization from the medium into *E. coli* cells. These findings strongly implicated Fe^{3+} as the activating signal for PmrAB under Pi depletion.

Given that *S. Typhimurium* PmrB (StPmrB) senses Fe^{3+} through conserved glutamic acid residues (E36, E39, E61, E64) in its periplasmic domain,⁴² we hypothesized a similar mechanism for *E. coli* PmrB (EcoPmrB). To test this, we generated chromosomal *pmrBE36A* and *pmrBE39A* mutations in *E. coli* MG1655 (Figure 4C [↗](#)). Consistent with their proposed role in Fe^{3+} sensing, these mutations abolished the *Parn-lacZ* reporter response to exogenous Fe^{3+} (100 μM) (Figure S10 [↗](#)). Crucially, both mutations also abolished *arn* operon upregulation under Pi depletion (Figure 4D [↗](#)), demonstrating that Pi depletion-induced PmrAB activation requires the Fe^{3+} sensing capability EcoPmrB.

To confirm the necessity of Fe mobilization, we observed that *arn* operon upregulation was abolished when cells were grown in Fe-free, Pi-depleted medium (Figure 4E [↗](#)). Although Pi depletion significantly impaired bacterial growth (doubling time increased from ~1 hr to ~6 hrs), co-depletion of Fe did not further exacerbate this effect, confirming that the observed PmrAB activation specifically responds to Pi-related Fe mobilization rather than general growth inhibition (data not shown). Investigating the sensitivity of this response, we found that reintroduction of Fe to Pi-depleted cells restored *Parn-lacZ* activity in a dose-dependent manner (Figure 4F [↗](#)), further confirming the role Fe mobilization in activating PmrAB and *arn* genes during Pi depletion. Importantly, *arn* activation in Pi-starved cells occurs at significantly lower exogenous Fe concentrations (~10-fold less) than in Pi-sufficient conditions (Figure 4F [↗](#)), suggesting an enhanced cellular capacity for Fe mobilization or sensing under Pi depletion.

Pi depletion triggers Mg^{2+} loss, leading to Fe^{3+} mobilization to membrane and PmrAB activation

To elucidate the mechanism of Fe mobilization during Pi depletion, we first investigated the role of canonical iron uptake pathways. Surprisingly, deletion of genes encoding outer membrane iron-chelator complex receptors and enterobactin synthetase (*fecA*, *fepA*, *fiu*, *cirA*, *entE*), individually or as a penta-deletion mutant ($\Delta 5\text{Fe}$), did not abolish *Parn-lacZ* induction during Pi depletion (Figure S11A [↗](#)). ICP-MS analysis further confirmed that cell-associated Fe still increased by over 5-fold in $\Delta 5\text{Fe}$ cells during Pi depletion (Figure S11B [↗](#)). These results indicated that Fe-mediated PmrAB activation during Pi depletion was independent of enhanced intracellular Fe uptake and suggested an alternative mechanism, likely involving Fe association with the cell surface, consistent with the known ability of PmrAB to sense periplasmic and surface-bound Fe^{3+} .⁴²

The outer leaflet of the Gram-negative outer membrane (OM) primarily consists of lipid A, whose negatively charged phosphate groups are typically neutralized by cell-associated Mg^{2+} and Ca^{2+} to maintain membrane stability.⁴⁷ Our ICP-MS analysis revealed a 44% reduction in cellular Mg content, while Ca^{2+} levels remained unchanged, in *E. coli* cells following 3 hours of Pi depletion treatment (Figure 4A [↗](#)). Monitoring the dynamics revealed that cellular Mg progressively decreased upon transferring *E. coli* cells to Pi-depleted medium, continuing over a 5-hour period (Figure 5A [↗](#)). This Mg^{2+} loss was independent of Fe, as a similar degree of loss occurred in Fe-free, Pi-depleted medium (Figure S12 [↗](#)). Conversely, cellular Fe increased, peaking after two hours of Pi depletion before slightly declining (Figure 5A [↗](#)). The temporal correlation between Fe accumulation and *Parn-lacZ* activity (Figure 5B [↗](#)) suggested active Fe mobilization to the cell surface during Pi depletion, potentially to compensate for Mg^{2+} loss and stabilize the membrane. The subsequent activation of the PmrAB-Arn system that remodel lipid A by decreasing negative charges, might thus represent an adaptive response to physiological changes, such as OM instability, caused by Mg^{2+} dissociation. Supporting this, deletion of *pmrA* led to an even greater and sustained increase in Fe mobilization during Pi depletion (Figure 5C [↗](#)), which could be toxic to *E. coli*.⁴²

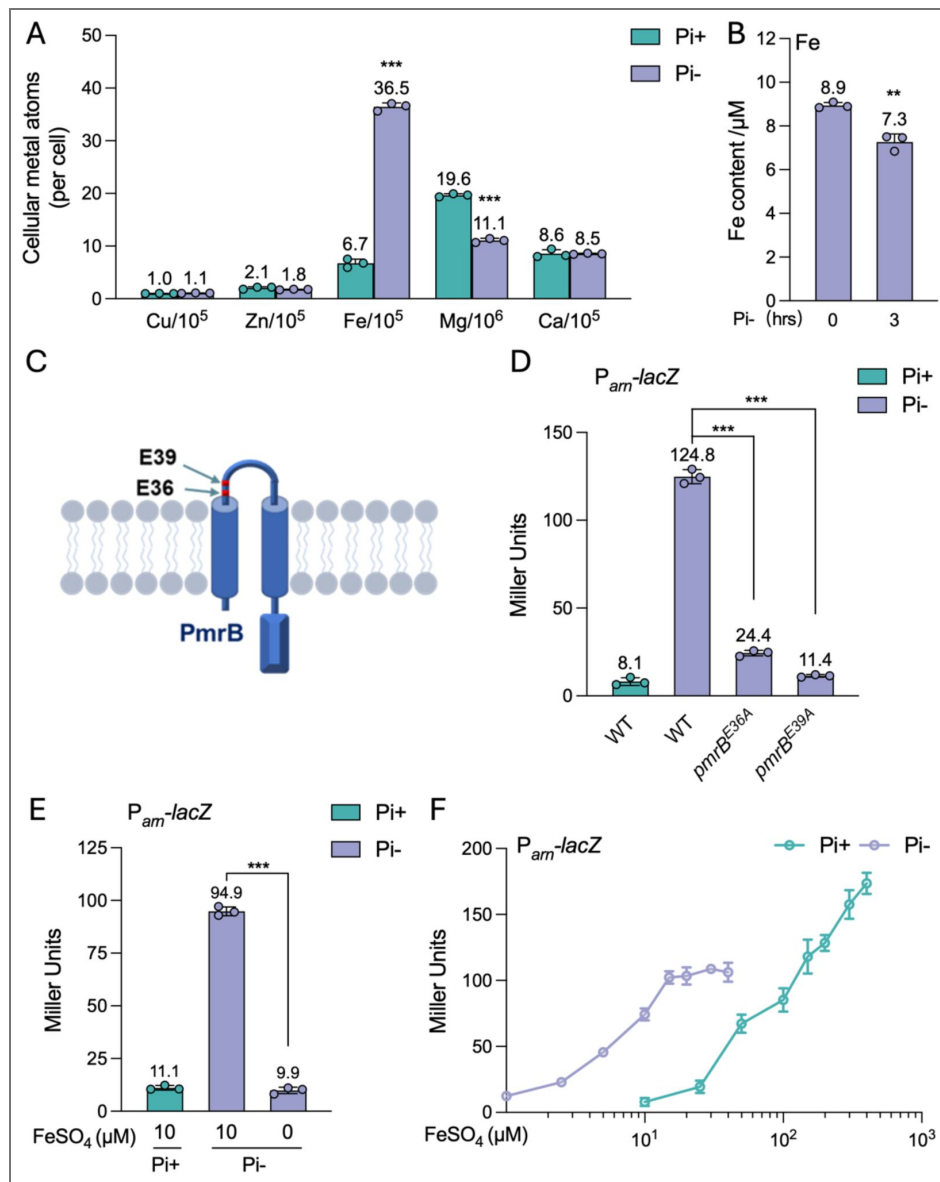


Figure 4. Activation of PmrAB during Pi depletion is mediated by the secondary stress signal iron (Fe³⁺) induced under this condition

(A) Cellular metal contents determined by ICP-MS in *E. coli* MG1655 cells following acute Pi-starvation treatment (Pi-, 0 mM) compared to the group without treatment (Pi+, 1.32 mM). (B) Iron contents in the spent medium of *E. coli* MG1655 at the indicated time points during Pi depletion treatment (Pi-, 0 mM). (C) Schematic diagram of the sensor kinase PmrB. Two important residues for sensing Fe³⁺, E36A and E39A, are shown. (D) β-galactosidase activities of *P_{arn}-lacZ* in MG1655 Δ *lacZ* parent and isogenic *pmrB*^{E36A} and *pmrB*^{E36A} mutants following acute Pi-starvation treatment (Pi-, 0 mM) compared to the group without treatment (Pi+, 1.32 mM). (E) β-galactosidase activities of *P_{arn}-lacZ* in MG1655 Δ *lacZ* cells following Pi depletion treatment (Pi-, 0 mM Pi, 10 μM Fe) or Fe, Pi depletion treatment (Pi- Fe-, 0 mM Pi, 0 μM Fe) compared to the group without treatment (Pi+, 1.32 mM Pi, 10 μM FeSO₄). (F) β-galactosidase activities of *P_{arn}-lacZ* in MG1655 Δ *lacZ* grown under Pi sufficient MOPS medium in the presence of different concentrations of FeSO₄ and that subjected to Pi depletion conditions in the presence of different concentrations of FeSO₄. Error bars represent the standard deviation of at least three independent experiments. Statistical significance was determined using one-way ANOVA followed by Dunnett's multiple comparisons test for B, and two-tailed Student's t-test for C, D, and E. Significance levels are indicated as follows: **p* < 0.05; ***p* < 0.01; ****p* < 0.001.

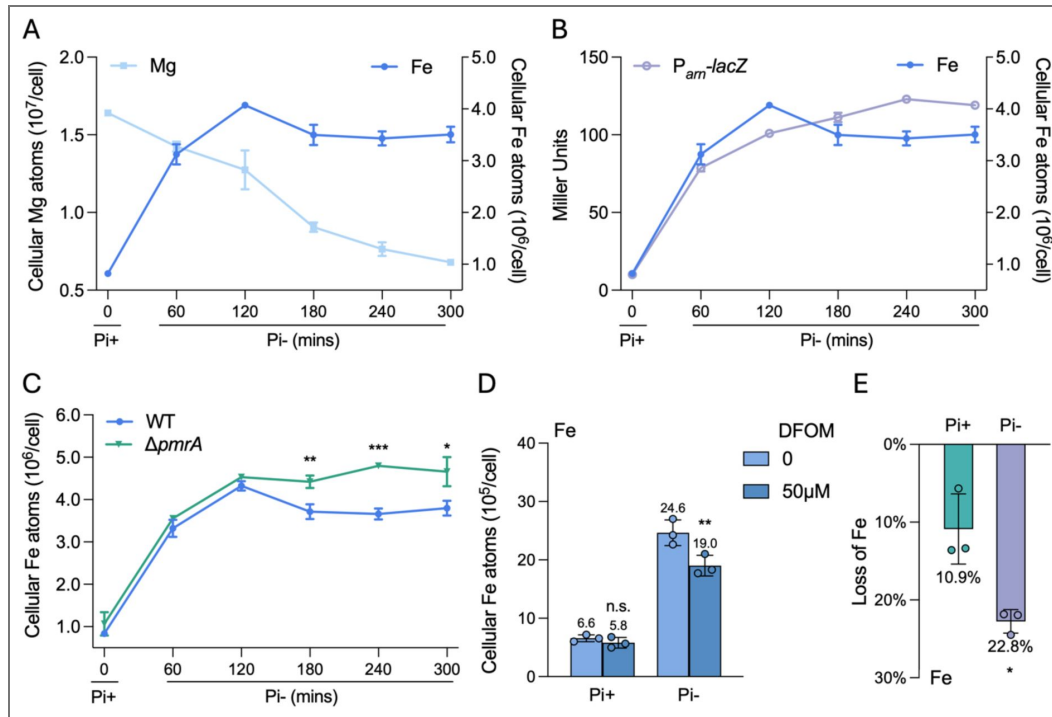


Figure 5. Response to Pi depletion induced iron mobilization to cell surfaces

(A) Iron (Fe) and magnesium (Mg) contents in *E. coli* MG1655 cells following Pi depletion treatment (Pi-, 0 mM Pi) at the indicated time points. (B) β -galactosidase activities of P_{arn} -lacZ in MG1655 Δ lacZ cells and Fe contents in *E. coli* MG1655 cells following Pi depletion treatment at the indicated time points. (C) Fe contents in *E. coli* MG1655 parent and isogenic Δ pmrA mutant cells following Pi depletion treatment (Pi-, 0 mM Pi) at the indicated time points. (D) Fe contents in *E. coli* MG1655 cells with Pi depletion treatment (Pi-, 0 mM) and without Pi depletion treatment (Pi+, 1.32 mM) following washing by HEPES or DFOM-supplemented (50μM) HEPES buffer. (E) Reduction of cellular Fe content following washing with DFOM-supplemented (50μM) HEPES buffer. Error bars represent the standard deviation of at least three independent experiments. Statistical significance was determined using two-tailed Student's t-test for C and E, and two-way ANOVA followed by Sidak's multiple comparisons test for D. Significance levels are indicated as follows: * $p < 0.05$; ** $p < 0.01$; *** $p < 0.001$.

To directly assess Fe association with the cell surface, we washed cell pellets with deferoxamine (DFOM)-containing buffer, a membrane-impermeable Fe³⁺-specific chelator.⁴⁸ ICP-MS analysis showed that washing with DFOM-supplemented buffer significantly reduced Fe content in cells treated with Pi depletion but had no significant effect on cells harvested from Pi-sufficient conditions (Figure 5D). Quantification revealed that Pi-starved cells exhibited a two-fold greater loss of Fe upon DFOM washing compared to Pi-sufficient conditions (Figure 5E), demonstrating that Pi depletion promoted Fe mobilization to cell surfaces, where it remained susceptible to removal by a membrane-impermeable chelator.

To uncover the driving force behind this enhanced Fe mobilization, we supplemented the culture medium with excess Mg (10 mM) to counteract Mg loss. This supplementation significantly reduced Fe mobilization to MG1655 cells during Pi depletion (Figure 6A); correspondingly, *P_{arn}-lacZ* activity declined as Mg concentration increased in the Pi-depleted medium (Figure 6B). These results strongly suggest that Fe mobilization to the cell surface during Pi depletion is dependent on Mg²⁺ loss. Further, monitoring Mg²⁺ dynamics in the spent medium revealed a continuous increase in Mg levels throughout the Pi depletion treatment (Figure 6C), confirming active Mg²⁺ dissociation from the cells. Similar Mg²⁺ release was observed even during combined Mg and Pi depletion (Figure S13). These results suggested that while Mg²⁺ is essential for bacterial growth, an imbalance with phosphorus during Pi depletion appears to trigger active Mg²⁺ dissociation from the cells. A comparable 45% Mg²⁺ loss was also observed in *P. aeruginosa* PAO1 under similar conditions (Figure S14). However, Fe mobilization was less pronounced (2.4-fold vs. 5.4-fold in *E. coli*), reflecting species-specific adaptation strategies.¹¹

Given that membrane-associated Mg²⁺ primarily neutralizes the negative charges of lipid A to stabilize the OM, we hypothesized that Mg²⁺ loss during Pi depletion alters OM properties, and Fe mobilization may serve to stabilize the OM. To test this, we employed an OM-sensitive probe.⁴⁹ The probe reports membrane surface properties through two orthogonal readouts: an overall fluorescence increase, which reflects probe disassembly upon binding to the anionic bacterial surface, and the pyrene excimer-to-monomer emission ratio (*I*₄₈₂/*I*₃₇₅), which captures differences in local surface interactions. The 2D sensor output revealed distinct signals between cells grown under Pi-sufficient and Pi-depleted conditions (Figure 6D), indicating altered OM characteristics. Notably, cells grown in Fe-free, Pi-depleted medium exhibited even greater shifts (Figure 6D), suggesting that Fe mobilization and subsequent activation of the PmrAB-Arn pathway served as an adaptation strategy to maintain OM integrity during Pi stress. This strategy likely prevents uncontrolled Fe accumulation and toxicity,⁴² ultimately resulting in stress-induced polymyxin resistance. A schematic model illustrating this process is presented (Figure 7).

Disrupting the Mg-Fe-PmrAB-Arn circuit counters Pi depletion-induced polymyxin resistance in *Enterobacteriaceae*

Our findings above identified a Mg-Fe-PmrAB-Arn circuit underpinning the polymyxin resistance induced by stress adaptation to Pi depletion. To evaluate whether interference with this pathway could mitigate the stress-induced polymyxin resistance, we supplemented Pi depletion medium with excess Mg²⁺ (10mM) or applied a membrane impermeable chelator DFOM (10μM). Both approaches effectively suppressed Pi depletion-induced polymyxin resistance in *E. coli* and *S. Typhimurium* (Figure 8A). In contrast, neither intervention reversed polymyxin resistance in *P. aeruginosa* despite various combinations of Mg²⁺ supplementation and Fe chelation (Figure S15). This highlights species-specific adaptive strategies and aligns with several observations from our study as well as several previous research.^{11,50} Specifically, in *P. aeruginosa*, despite a 45% Mg loss during Pi depletion, Fe levels increased only two-fold compared to over five-fold in *E. coli*, consistent with its reliance on MGDG/GADG lipids synthesis regulated by the PhoBR system (Figure 8B).¹¹ Additionally, *P. aeruginosa* exhibits a distinct lipid A modification, 2-hydroxy myristate (Figure S4D), that does not confer polymyxin resistance.⁵¹ Phylogenetic analysis of 250 PmrB homologs revealed that EcoPmrB and PaePmrB cluster in separate clades, with PaePmrB lacking the conserved “ExxE” motif essential for Fe³⁺ sensing (Figure 8C). Together, these

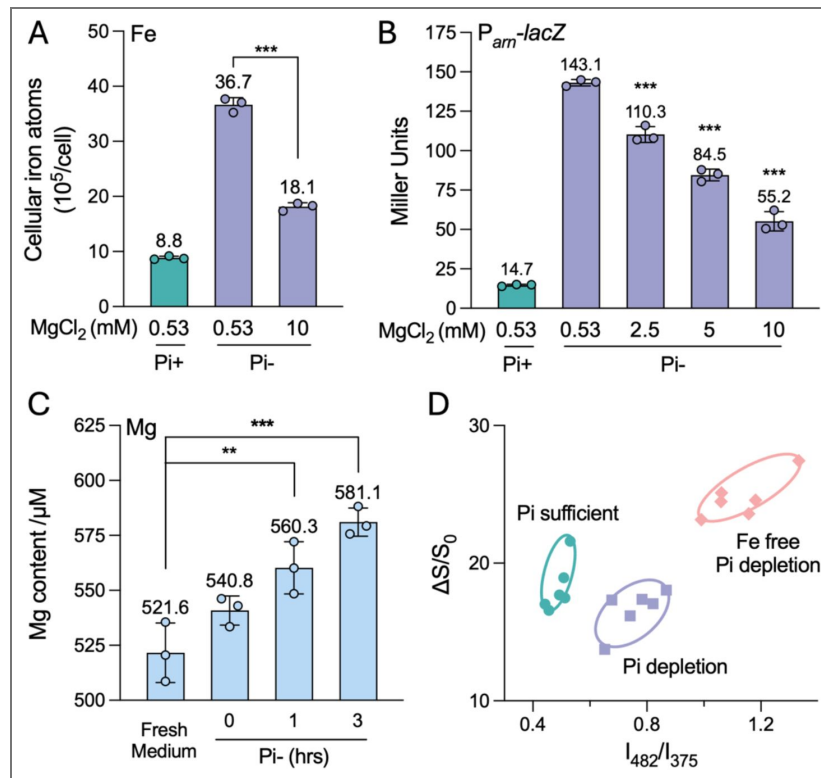


Figure 6. Iron mobilization is driven by Mg^{2+} dissociation during Pi depletion

(A) Fe contents in *E. coli* MG1655 cells following acute Pi-starvation treatment (Pi-, 0 mM Pi, 0.53 mM Mg) or Mg excess Pi depletion treatment (Pi-, 0 mM Pi, 10 mM Mg) compared to the group without treatment (Pi+, 1.32 mM, 0.53 mM Mg). (B) β -galactosidase activities of P_{arn} -*lacZ* in MG1655 Δ *lacZ* cells following acute Pi-starvation treatment (Pi-, 0 mM Pi, 0.53 mM Mg) or Mg excess Pi depletion treatment (Pi-, 0 mM Pi, 10 mM Mg) compared to the group without treatment (Pi+, 1.32 mM, 0.53-10 mM Mg). (C) Mg content in the spent medium during Pi depletion treatment at the indicated time points. (D) 2D graph plotted from output signals of two channels of the PI-BactD sensor: fluorescence increase ($\Delta S/S_0$) and fluorescence radiometric changes (I_{482}/I_{375}) in each of the treatments indicated. Data are presented as mean \pm s.d. of three biological replicates for A, B, and C, and six biological replicates for D. Error bars represent the standard deviation of at least three independent experiments. Statistical significance was determined using two-tailed Student's t-test for a, and one-way ANOVA followed by Dunnett's multiple comparisons test for B and C. Significance levels are indicated as follows: * $p < 0.05$; ** $p < 0.01$; *** $p < 0.001$.

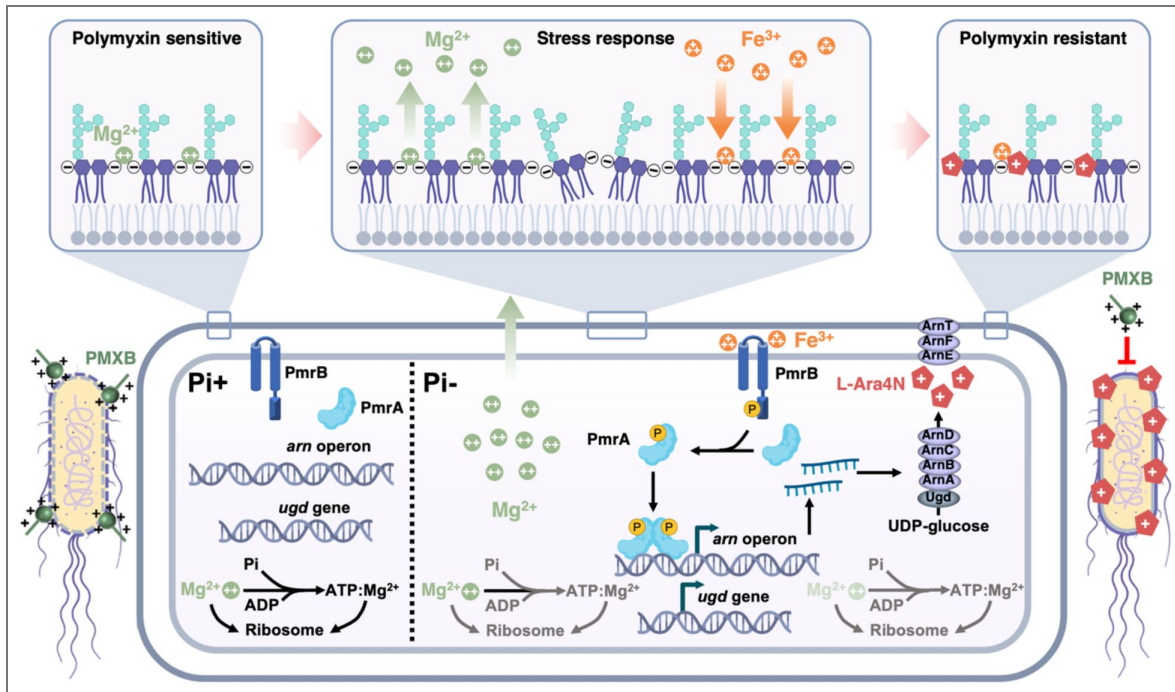


Figure 7. A Mg-Fe-PmrAB regulatory circuit underpins the Pi-depletion induced polymyxin resistance through activating the lipid A L-Ara4N modification system

In cell grown under Pi sufficient condition, ribosome and ATP serve as the major intracellular Mg^{2+} and Pi reservoir. Mg^{2+} neutralizes negative charge of lipid A and stabilizes outer membrane (OM). The PmrAB two-component system (TCS) is inactive, and the cell is sensitive to polymyxin. During Pi stress, ATP biosynthesis and ribosome biogenesis are halted due to Pi depletion, disrupting the balance between Pi and Mg^{2+} . Mg^{2+} disassociates from the cell which destabilizes the OM and derives compensatory Fe^{3+} mobilization to cell surface. Mobilized Fe^{3+} activates the PmrAB TCS which in turn upregulates the *arn* operon. Arn and Ugd proteins catalyze the biosynthesis of L-Ara4N and modify lipid A with L-Ara4N to stabilize OM under stressed condition and prevent further Fe mobilization. *E. coli* cells with L-Ara4N modified lipid A become resistant to polymyxin.

findings underscore the diverse stress response strategies employed by different classes of Gram-negative bacteria and highlight the importance of understanding species-specific regulatory mechanisms for developing targeted interventions against stress-induced antibiotic resistance.

Discussion

Bacterial adaptation to environmental stressors is crucial for survival and pathogenesis. Phosphate (Pi) scarcity, a pervasive condition in diverse environments including host-associated niches such as macrophage phagosomes, salmonella-containing vacuoles, and cystic fibrosis sputum, is a potent cue driving antimicrobial resistance (AMR) against cationic antibiotics such as polymyxins.^{9–11} Adaptive mechanisms previously characterized for Pi depletion-induced AMR often involve remodeling bacterial membranes by substituting phosphorus-containing phospholipids with Pi-free, neutral, or positively-charged lipids.^{11,26–28} However, the specific mechanisms in clinically important Enterobacteriaceae, which largely lack these canonical phospholipid remodeling pathways, have remained largely unknown. In this study, we unveil a conserved, yet distinct, polymyxin B resistance mechanism in *Enterobacteriaceae*: Pi limitation triggers a cascade of cationic imbalance and Fe³⁺ signaling, leading to L-Ara4N modification of lipid A and outer membrane remodeling, a process distinct from phospholipid-based resistance pathways (Figure 7). This intricate Mg-Fe-PmrAB regulatory circuit represents a previously unappreciated ecophysiological vulnerability, offering a novel strategy to mitigate stress-induced polymyxin resistance.

Maintaining a balanced P/Mg ratio is paramount for bacterial cellular physiology, with ATP and rRNA serving as primary cytoplasmic reservoirs for both Pi and Mg²⁺.^{52–55} Previous work by Bruna et al. demonstrated that bacteria suppress Pi uptake under Mg²⁺ limitation to preserve cellular function.⁵³ Herein, our study extends this understanding by showing that Pi scarcity itself actively triggers Mg²⁺ release from *E. coli* cells. This observation underscores the tightly coupled nature of Pi and Mg²⁺ homeostasis. Our comprehensive proteomic analysis further supports this, revealing that proteins involved in translation, ribosomal structure, and biogenesis were among the most significantly downregulated groups during Pi depletion (Figures 1A and S3). Concurrently, we observed a steady decline in cellular ATP levels under Pi-limited conditions (Figure S16), suggesting a profound arrest in ribosome biogenesis and protein synthesis that likely contributes to the observed Mg²⁺ release and cellular loss.

In *Enterobacteriaceae*, Mg²⁺ homeostasis is primarily governed by the PhoPQ two-component system, which is well-characterized in *S. Typhimurium* to be activated under low extracellular Mg²⁺ conditions.^{56,57} Given the observed Mg²⁺ release during Pi-depletion, we investigated the involvement of this classical Mg²⁺-sensing PhoPQ system. Our results showed that despite cellular Mg²⁺ loss during Pi depletion, the transcription of key PhoPQ regulon genes, such as *phoQ* and *mgtA*, remained unchanged (Figure S17). This indicates that while cellular Mg²⁺ levels are perturbed, they do not drop sufficiently to activate the canonical PhoPQ response. Instead, our data compellingly demonstrate that under acute Pi depletion, *Enterobacteriaceae* preferentially engage an alternative, Fe³⁺-mediated membrane remodeling pathway. This pathway activates the *arn* operon and subsequent L-Ara4N modification independently of the classical Mg²⁺-sensing PhoPQ system, highlighting a distinct adaptive strategy.

This Fe³⁺-mediated lipid A modification strategy in *Enterobacteriaceae* offers a stark contrast to Pi depletion-induced polymyxin resistance mechanisms described in other Gram-negative bacteria, notably *P. aeruginosa*. In *P. aeruginosa*, Pi depletion primarily activates the PhoBR regulon, orchestrating the biosynthesis of phosphorus-free glycolipids (MGDG and GADG) to replace negatively charged phospholipids and maintain membrane integrity (Figure 8B).¹¹ While *P. aeruginosa* possesses a PmrAB homolog, its PmrB sensor kinase lacks the critical Fe³⁺-sensing “ExxE” motifs found in *Enterobacteriaceae* PmrB, precluding direct Fe³⁺ response. Instead, PmrAB activation in *P. aeruginosa* is typically coupled to the PhoPQ system, which senses low extracellular Mg²⁺. Thus, while *P. aeruginosa* employs PhoBR-regulated phospholipid remodeling as its primary Pi depletion response, *Enterobacteriaceae*, largely lacking these glycolipid pathways, have evolved to utilize a secondary, Fe³⁺-sensing mechanism. Here, the PmrAB system, via its specific Fe³⁺-

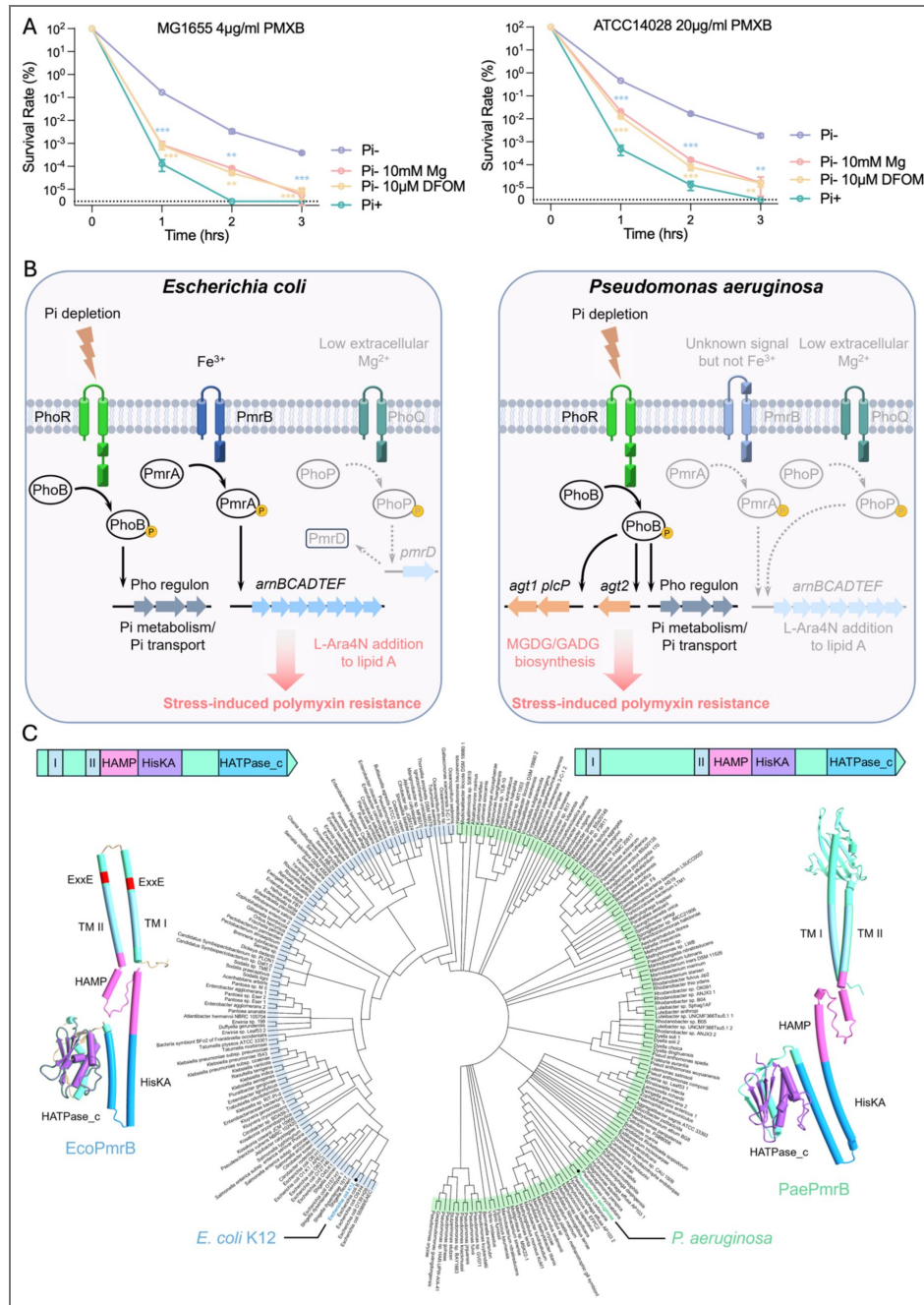


Figure 8. Disrupting the Mg-Fe-PmrAB signaling circuit abolished Pi-depletion induced polymyxin resistance in *Enterobacteriaceae*

(A) Time-kill curves of *Escherichia coli* MG1655 (left panel) and *Salmonella Typhimurium* ATCC14028 (right panel) exposed to polymyxin B (PMXB) (4 μg/ml for *E. coli* strains, 20 μg/ml for *S. Typhimurium*) following acute Pi-starvation treatment (Pi-, 0 mM Pi), Pi depletion treatment with excess Mg (Pi-, 0 mM Pi, 10mM MgCl₂) or Pi depletion treatment with iron chelator (Pi-, 0 mM Pi, 10 μM DFOM) compared to the group without treatment (Pi+, 1.32 mM Pi). (B) Distinct stress adaptation strategies in *E. coli* and *P. aeruginosa* under Pi depletion conditions. Genes and regulatory systems activated in the two species are illustrated. Inactive regulatory systems are depicted in faded effects. The regulatory mechanisms for *P. aeruginosa* are based on findings from Jones et al.¹¹. (C) A phylogenetic tree of 250 PmrB homologous. A predominant clade is indicated by a blue circle, comprising sequences from bacteria such as *Escherichia*, *Shigella*, *Citrobacter*, *Salmonella*, *Klebsiella*, *Yersinia*, and *Enterobacter* species. A green circle marks several clades distinct from the predominant one. The domain architecture and AlphaFold3-predicted structure of EcoPmrB and PaePmrB are shown. Error bars represent the standard deviation of at least three independent experiments. Statistical significance was determined using one-way ANOVA followed by Dunnett's multiple comparisons test. Significance levels are indicated as follows: **p* < 0.05; ***p* < 0.01; ****p* < 0.001.

sensing “ExxE” motifs in PmrB, orchestrates membrane remodeling through L-Ara4N modification of lipid A as a key physiological adaptation to Pi depletion.⁵⁰ While *P. aeruginosa* also exhibits lipid A modification (e.g., 2-hydroxymyristate by LpxO) during Pi depletion, this modification does not contribute to polymyxin resistance and is regulated independently of PhoBR, PhoPQ, or PmrAB, highlighting distinct physiological roles.⁵¹

The biosynthesis of L-Ara4N and its transfer to lipid A are mediated by Ugd and ArnABCDEFT proteins, encoded by the *ugd* gene and the *arn* operon, respectively.^{58–61} Our data reveal a sophisticated regulatory separation: during Pi depletion, *arn* transcription is tightly controlled by the PmrAB system, while *ugd* expression is not PmrAB-dependent and exhibits partial regulation by the PhoBR system (Figure S6 [↗](#)). This bifunctional control is not unexpected, as *ugd* encodes UDP-glucose dehydrogenase, an enzyme with dual roles in L-Ara4N biosynthesis and in the production of exopolysaccharides like colanic acid.^{62,63} Therefore, while PmrAB activation of *arn* is absolutely critical for L-Ara4N modification of lipid A during Pi limitation, *ugd* regulation reflects its broader involvement in diverse cellular metabolic and stress responses.

While preparing this manuscript, a recent study by Baijal et al. (2024) reported that the *ppk* gene modulates *arn* operon upregulation under combined nutrient limitations (transfer from rich LB to low-Pi, no-amino-acid MOPS medium) in *E. coli*.⁶⁴ Inspired by this, we investigated the role of *ppk* in polymyxin resistance specifically under Pi depletion, our primary focus. We found that *ppk* deletion did not affect *arn* or *ugd* promoter activity under sole Pi-depleted conditions (Figure S18 [↗](#)), indicating its dispensability when Pi is the only limiting factor. To reconcile these findings, we replicated the Baijal et al. experimental conditions, confirming *ppk*-dependent *arn* upregulation under combined Pi and amino acid scarcity (Figure S19A [↗](#)). Our subsequent experiments, systematically disentangling these stresses, revealed that while both Pi and amino acid depletion induce *arn* upregulation, Pi depletion is the dominant driver, and *ppk*-dependent regulation emerges only under combined Pi and amino acid scarcity (Figure S19B [↗](#)). These results clarify that while *ppk* influences *arn* expression under specific multifactorial stresses, our identified PmrAB-*arn* pathway is independently and dominantly activated by Pi depletion alone, providing precise mechanistic insight into this fundamental environmental stressor.

In both natural habitats and host-associated niches, Pi scarcity imposes dual challenges: nutrient acquisition and defense against antimicrobial threats. The Pi-Mg-Fe-PmrAB regulatory circuit we have uncovered likely represents a sophisticated adaptive strategy for *Enterobacteriaceae*, facilitating their survival in highly heterogeneous environments with fluctuating Pi levels, such as during host colonization, transmission, or environmental persistence.⁶⁵ This PmrAB-mediated membrane remodeling not only confers resistance to polymyxins but may also enable bacteria to preserve membrane integrity and withstand other cationic antimicrobial peptides (CAMPs) produced by competing microbes or host defenses.

In summary, our findings elucidate a conserved yet distinct regulatory circuit in *Enterobacteriaceae* that intricately links Pi and Mg²⁺ homeostasis to Fe³⁺-mediated lipid A modification, driving stress-induced antibiotic resistance. This mechanism is notably distinct from those characterized in *P. aeruginosa* or *A. baumannii*. Crucially, we demonstrate that targeting this circuit effectively mitigates stress-induced resistance. Given that polymyxins remain indispensable as last-line antibiotics for treating multidrug-resistant Gram-negative bacterial infections, our study not only offers critical insights into the fundamental molecular mechanisms underlying stress-induced resistance but also highlights a promising avenue for informing novel resistance management strategies.

Materials and methods

Bacterial strains and growth conditions

Strains, plasmids, and primers used in this study are listed in the S2 [↗](#) and S3 Tables [↗](#). Bacteria were cultured in lysogeny broth (LB) broth/plates or MOPS minimal medium. MOPS medium was freshly prepared from 1× MOPS stock by supplementing 0.1 % (w/v) glucose and 1.32 mM K₂HPO₄. Acute Pi depletion was applied by transferring bacteria culture into the non-Pi MOPS medium. 1×

MOPS consists of 40 mM MOPS, 4 mM Tricine, 10 μM $\text{FeSO}_4 \cdot 7\text{H}_2\text{O}$, 9.5 mM NH_4Cl , 0.276 mM K_2SO_4 , 0.5 μM $\text{CaCl}_2 \cdot 2\text{H}_2\text{O}$, 525 μM MgCl_2 , 50 mM NaCl, 0.003 μM $(\text{NH}_4)_6\text{Mo}_7\text{O}_{24}$, 0.4 μM H_3BO_3 , 0.03 μM CoCl_2 , 0.01 μM CuSO_4 , 0.08 μM MnCl_2 , and 0.01 μM ZnSO_4 . Antibiotics applied to select and maintain the construct were chloramphenicol (25 $\mu\text{g}/\text{ml}$), kanamycin (20 $\mu\text{g}/\text{ml}$) and ampicillin (100 $\mu\text{g}/\text{ml}$).

Lipid A extraction and ESI-MS analysis

Lipid A was extracted from designated *E. coli* cells using Bligh-Dyer method as described with minor modifications.⁶⁶ *E. coli* MG1655 cultured in MOPS medium to OD_{600} of 0.5 was harvested as cells under Pi sufficient condition. The same volume of cells was washed with Pi depletion medium for 3 times and resuspended in Pi depletion medium and shake for 3 hrs at 37°C as cells subjected to Pi depletion. 200 ml of each type of cell pellets with three biological replicates were harvested by centrifugation at 4500 rpm for 30 min and washed with H_2O . The cell pellets were suspended in 76 ml of a single-phase Bligh-Dyer mixture (chloroform: methanol: water=1:2:0.8; v/v/v) and stirred at room temperature for 1 h. Insoluble debris was collected by centrifugation at 4500 rpm for 30 min, washed with 60 ml single-phase Bligh-Dyer mixture, and suspended in 27 ml of 12.5 mM sodium acetate (pH 4.5). The mixture was heated at 100°C for 30 min and cooled to room temperature. The suspension was mixed with 30 ml chloroform and 30 ml methanol. Following vigorously shaken for extraction of lipid A and centrifugation for 30 min, the lower phase containing lipid A was collected and dried with a rotary evaporator.

All the mass spectra of lipid A samples were acquired using Waters SYNAPT quadrupole time-of-flight mass spectrometer (MS) equipped with an electrospray ionization source.⁶⁷ Lipid A samples were dissolved in a mixture of chloroform and methanol (4 : 1; v/v) and subjected to ESI/MS in the negative ion mode. Data acquisition and analysis were performed using MASS LYNX V4.1 software, Waters, Milford, MA, USA.

ICP-MS and DFOM treatment

Total cellular metal content was quantified using inductively coupled plasma mass spectrometry (ICP-MS) following previous description with minor modifications.⁶⁸ *E. coli* cells equivalent to OD_{600} as 5 were harvested by centrifugation at 4500 rpm for 15 mins and washed three times with ice-cold PBS buffer. Cell pellets were subjected to acid digestion with 100 μl 65.0 % HNO_3 (Fluka) at 65°C for 16hrs. Samples were diluted to a final volume of 15 ml with 1% HNO_3 and subjected to ICP-MS detection on Agilent 7900 system (Agilent Technologies, CA). Samples were further diluted if the signals exceeded the linear range of standard curve. The standard curves of tested metals were generated from multi-element calibration standard-2A for ICP-MS (Agilent). Metal contents in bacteria were calculated based on the standard curve and results were normalized to original cell number.

Deferoxamine mesylate salt (sigma) were applied to examine the degree of iron association to *E. coli* cell surface. *E. coli* cells equivalent to OD_{600} as 5 were harvested by centrifugation at 4500 rpm for 15 mins. Cell pellets were resuspended in HEPES buffered saline with and without 50 μM DFOM and incubated in 37°C for 30 mins with 220rpm agitation. Total cellular metal content of these treated cells was quantified using inductively coupled plasma mass spectrometry (ICP-MS) as described above.

OM feature monitoring using PI-BactD

OM feature of *E. coli* was monitored by an OM-sensitive probe PI-BactD following previous description with minor modifications.⁴⁹ *E. coli* cells grown under designated conditions were harvested by centrifugation at 13000 rpm for 2 mins and washed with PBS buffer (10 mM, pH 7.2) twice. Cell pellets were resuspended in PBS buffer to an OD_{600} of 0.5. Fluorescence probe PI-BactD (gift from prof. Xu Z, Dalian) was added into 1mL cell suspension to a final concentration of 2 mM and incubated at room temperature for 1 min. Output signals of two channels: fluorescence

increase ($\Delta S/S_0$) and fluorescence ratio metric changes (I_{482}/I_{375}) were recorded to plot the 2D graph (Thermo Scientific Varioskan® Flash spectral scanning multimode reader). Six replicates were conducted for each strain and treatment.

Construction of Ppromoter-*lacZ* (*Parn-lacZ* as example) fusion in the single-copy plasmid pNN387

A DNA fragment corresponding to the -200 to -1 region relative to the ATG start codon of *arnB* was amplified using *E. coli* MG1655 genomic DNA as the template and primers specific to this fragment flanked with NotI and HindIII restriction sites at the 5'- and 3'-end, respectively. Following digestion with NotI and HindIII and purification using the MiniBEST agarose gel DNA extraction kit (TaKaRa), the fragment was ligated into the plasmid pNN387 which was treated with the same restriction enzymes using the quick ligation kit (NEB). The resulting construct was selected on LB agar plates supplemented with chloramphenicol (25 µg/ml) and was verified by DNA sequencing (BGI, Shenzhen).

Beta-galactosidase activity assay

β-gal activity assay was performed based on a previous description with modifications.⁶⁸ Cells were grown under designated conditions until OD_{600} reached 0.4. 10 µg/ml tetracycline was added to stop cell growth and protein synthesis, and cells were left on ice until being assayed. 100 µl of cell culture and 400 µl of Z buffer (60 mM Na_2HPO_4 , 40 mM NaH_2PO_4 , 10 mM KCl, 1 mM $MgCl_2$, 50 mM β-mercaptoethanol, pH 7.0, 4 °C) were mixed. One drop of 0.1% SDS and two drops of chloroform were added to lyse the cells. The reactions were initiated by adding 100 µl of 4 mg/ml ortho-nitrophenyl-β-galactoside into cell suspension and were incubated at 28 °C. Color development in the mixtures was monitored. Finally, 250 µl of 1M Na_2CO_3 was added to stop the reaction. Color of the mixtures were measured using spectrophotometer at OD_{420} and OD_{550} . The expression value in Miller units was calculated, and results are presented as the mean of three biological replicates.

RNA extraction and RT-qPCR

Bacterial cells grown under designated conditions was subjected to RNA extraction when the OD_{600} reached 0.4. Cells were harvested by centrifugation at 4,500 rpm for 10 min at 4 °C. After removing the supernatant, the cell pellet was stored at -80 °C to aid cell lysis. Total RNA was extracted using the MiniBEST Universal RNA Extraction Kit (Takara, Japan) according to the manufacturer's instruction. Reverse transcription (RT) was performed using PrimeScript™ RT reagent Kit (Takara, Japan). Quantitative PCR was performed using specific primers and the TB Green® Premix Ex Taq™ (Takara, Japan) in a 20 µL reaction system. The reaction was performed in the ABI StepOnePlus real time PCR system with *rrsB* as reference gene to normalize the relative expression of the target genes. The results were presented as fold change expression of the target genes, and results were presented as the mean of three biological isolates.

Construction of clean gene deletion, point mutation and tag insertion in chromosome of *E. coli* MG1655

Gene deletion, mutation, and tag insertion in chromosomal were achieved employing a CRISPR/Cas9-mediated approach developed by Zhao et al. with modifications.⁶⁹ For gene deletion (deletion of *lacZ* as example), *E. coli* MG1655 was electrotransformed with pCAGO plasmid which contains both SpCas9 and λ-RED to obtain MG1655-pCAGO. A single colony of the resulting transformant was inoculated into LB medium supplemented with ampicillin (100 mg/ml) and grew overnight at 30°C. 100 µl of the overnight culture was inoculated into 10 ml fresh culture medium and cells were grown at 30°C with IPTG (0.1 mM) induction to OD_{600} as 0.6. The cells were collected and washed with cold ddH₂O for three times, generating competent cells for electroporation. An aliquot comprising 100 µl competent cells was mixed with 800 ng of the editing-cassette which encompasses 40 bp of sequence among the CDS of *lacZ* gene followed by the

chloramphenicol resistant gene, the N20PAM sequence (GTCCATCGAACCGAAGTAAGG), 40 bp upstream-homologous arm of *lacZ* gene, and 40bp downstream-homologous arm of *lacZ* gene, in a 2 mm Gene Pulser cuvette (Bio-Rad) and was subjected to electroporation at 2.3 kV. Following recovering the transformants by cultivation in LB medium for 2 hrs at 30°C, the mixture was spread onto LB agar plate supplemented with ampicillin (100mg/ml), chloramphenicol (25 mg/ml), and 1% glucose (to avoid the background expression of the Cas9 protein). Single colonies were collected and verified by colony PCR to obtain an authentic clone in which the editing-cassette was embedded in chromosomal. The confirmed colony was inoculated into LB medium supplemented with ampicillin (100 mg/ml), IPTG (0.1 mM), and L-arabinose (0.2%) at 30°C overnight to enable expression of SpCas9 and the λ -RED recombinase. The cells were then streaked on LB agar plates supplemented with ampicillin (100mg/ml). Following colony PCR, desired colonies containing deletion of the *lacZ* gene were verified by DNA sequencing (BGI, Shenzhen). For point mutation, (mutation of *pmrB* E36 to A as example) *E. coli* MG1655 was conducted following the same procedures except for the editing cassette sequence which encompasses 40 bp of upstream-homologous arm of GAA (Glu36) followed by the chloramphenicol resistant gene, the N20PAM sequence, the 40 bp upstream-homologous arm of GAA (Glu36), GCA (Ala) and 40 bp downstream-homologous arm of GAA (Glu36). For tag insertion, (insertion 3xFLAG to C-terminal of *arnB* gene as example) *E. coli* MG1655 was conducted following the same procedures except for the editing cassette sequence which encompasses 40 bp of upstream-homologous arm of stop codon of *arnB* gene followed by the chloramphenicol resistant gene, the N20PAM sequence, the 40 bp upstream-homologous arm of stop codon of *arnB* gene, tag sequence and 40 bp downstream-homologous arm of stop codon of *arnB* gene (include stop codon). After obtaining all desired genome modifications, the editing plasmid was cured by growing the resulting cells at 42°C for 48 hrs.

Construction of pET28A-pBAD-*pmrA* for PmrA protein expression

A DNA fragment encoding the PmrA protein was amplified using genomic DNA of *E. coli* MG1655 as the template and primers specific to this fragment flanked with NcoI and XhoI restriction sites at the 5'- and 3'-end, respectively. After digestion with NcoI and XhoI, and purification using the MiniBEST agarose gel DNA extraction kit (TaKaRa), the purified fragment was ligated into the plasmid pET28a-pBAD and pET28a-pBAD-3xFLAG⁴³ which was treated with the same restriction enzymes using the quick ligation kit (NEB). The resulting construct was selected on LB agar plates supplemented with kanamycin (20 μ g/ml) and was verified by DNA sequencing (BGI, Shenzhen). All plasmids constructed are listed in the supplementary S3 Table.

Immunoblot analysis

Protein levels of ArnB and PmrA were analyzed by SDS-PAGE following Western Blot. 1ml of cells with OD₆₀₀ of 0.5 was collected and resuspended in 200 μ l sample buffer (13 mM Tris, 0.2% SDS, 5% glycerol, 0.004% bromophenol blue, pH 6.8) before being subjected to cell lysis by sonication. Following centrifugation at 13000 rpm for 10 min at 4°C, 20 μ l of the sample was separated on SDS-PAGE gels (TGX FastCast Acrylamide Kit, 10%, BIO-RAD). Proteins were then transferred onto a polyvinylidene difluoride (PVDF) membrane (BIO-RAD) using a Trans-Blot SD Semi-Dry Transfer Cell (BioRad) at constant voltage (25 V) for 7 min. Membranes were blocked for 1 h with 5% non-fat milk solution in TBST (20 mM Tris, 150 mM NaCl, 0.1% Tween-20) at room temperature followed by incubation with 1:10,000 primary antibody (monoclonal or polyclonal anti-His antibody) in 1% non-fat milk in TBST at room temperature with shaking for 1 hour. After washing with TBST, the membrane was incubated with the secondary antibody (Goat anti-mouse IgG HRP conjugate) in 1% non-fat milk in TBST at room temperature with shaking for 1 hour. Chemiluminescence of protein bands was detected by ECL Plus Western Blotting Detection Reagents (GE Healthcare, USA), and imaged using a X-ray film development by Alliance Q9 (UVITEC, United Kingdom).

Phos-tag SDS-PAGE

In vivo phosphorylation of PmrA was examined using Phos-Tag SDS-PAGE following our previous description with minor modifications.⁴³ *E. coli* MG1655 Δ *pmrA* cell harboring pET28a-pBAD-*pmrA*-3 \times FLAG (AY7068) was inoculated into MOPS minimum medium supplemented with kanamycin (20 μ g/ml) and grew overnight at 37°C. 100 μ l of the overnight culture was inoculated into 5 ml fresh MOPS medium and grew at 37°C for 4 hrs. Expression of PmrA was induced with 1mM L-arabinose for 1 hr. Cells were collected by centrifugation at 13000 rpm and were washed with MOPS medium supplemented with 0.1, 0.5, or 1 mM FeSO₄ or Pi- MOPS medium twice and shake for 1 hr at 37°C in the corresponding medium. 1ml of cells with OD₆₀₀ of 0.5 was collected for the subsequent analysis. Cell pellet was washed with cold PBS twice and was resuspended in 200 μ l sample buffer (13 mM Tris, 0.2% SDS, 5% glycerol, 0.004% bromophenol blue, pH 6.8) before being subjected to cell lysis by sonication. Following centrifugation at 13000 rpm for 10 min at 4°C, 20 μ l of the sample was loaded onto a 10% Tris-Gly polyacrylamide gel containing 25 mM Phos-tag Acrylamide (Wako) and 50 mM MnCl₂. Samples were separated by electrophoresis for 2 hrs at 4°C, following washing with 50 ml transfer buffer containing 10 mM EDTA for 20 min to remove residual Mn²⁺. Proteins on the gel were transferred onto a PVDF membrane. The membrane was blocked with 5% non-fat milk in TBST buffer and was incubated subsequently with monoclonal ANTI-FLAG[®] M2 antibody (Sigma) and goat anti-mouse IgG (H+L)-HRP conjugate (Bio-rad). To detect FLAG-tagged protein bands, the membrane was submerged in the ECL Plus Western Blotting Detection Reagents (GE Healthcare) for 2 min and then subjected to the imaging system (UVITEC Cambridge) to record signals.

Amber codon mutation of selected CouA incorporation sites in pET28A-pBAD-*pmrA*

Selective amino acid located in the DNA binding domain of PmrA was subjected to replacement by CouA, each of these CouA incorporation sites were mutated to a TAG amber codon by site-directed mutagenesis PCR. PCR was conducted using a pair of primers for the desired mutagenesis and pET28A-pBAD-*pmrA* plasmid as the template. PCR product was purified using MiniBEST agarose gel DNA extraction kit (TaKaRa). Following DpnI digestion of the template for 16 hrs, the PCR product was transformed into *E. coli* DH5 α . Transformants were recovered on LB agar plates supplemented with kanamycin (20 μ g/ml) at 37°C overnight. Colonies recovered were verified by DNA sequencing (BGI, Shenzhen).

In vivo PmrACouA - promoter_{SYTO 9} binding assay

Binding of PmrA_{CouA} and promoter_{SYTO 9} was monitored by FRET assay following our previous description with minor modifications.⁴³ Plasmid pET28a-pBAD-*pmrA*-G137TAG was co-transformed with pEVOL-CouRS into *E. coli* MG1655 Δ *pmrA* strain, resulting in AY7065 constructs. A fresh single colony of AY7065 was inoculated into MOPS medium supplemented with kanamycin (20 μ g/ml) and chloramphenicol (25 μ g/ml) and grew overnight at 37°C. 75 μ l of the overnight culture was inoculated to 7.5 ml fresh medium to subculture the bacteria. Following culturing at 37°C for 4 hrs, CouA incorporation and expression of PmrA-G137CouA was induced mildly by supplementing 0.9% arabinose and 1mM CouA at 37°C for 5 hrs. Approximately 3.5 \times 10¹⁰ cells were harvested and washed twice with fresh MOPS medium. Cells were resuspended in MOPS medium as control, or MOPS medium supplemented with 0.5 mM FeSO₄, or Pi- MOPS medium and shake for 1 hr at 37°C. After centrifugation at 4500 rpm for 15 min at 4°C, cell pellet was resuspended in 600 μ l of PBS. 85 μ l of the suspension was added in each of 6 wells (3 wells for control and 3 wells for experimental group) on a 96-well black plate preloaded with 15 μ l of 50 μ M SYTO 9 and was incubated for 15 min at room temperature in the dark before being subjected to fluorescence recording (Thermo Scientific Varioskan[®] Flash spectral scanning multimode reader).

Comparative proteomic analysis

E. coli MG1655 cultured in MOPS medium to OD₆₀₀ of 0.5 was harvested as cells under Pi sufficient condition. The same volume of cells was washed with Pi depletion medium for 3 times and resuspended in Pi depletion medium and shake for 3 hrs at 37°C as cells subjected to Pi depletion. Each type of cell pellets with three biological replicates were lysed by resuspending in 20 µl BugBuster reagent (Novagen, USA) (containing 25 mg/ml lysozyme, 1 unit DNase I) at room temperature for 30 mins following centrifugation at 13000 rpm at 4°C for 20 min. Supernatant was transferred to a clean microcentrifuge tube and mixed with 4×SDS sample buffer (40% glycerol, 8% SDS, 240 mM Tris/HCl pH 6.8, 0.04% bromophenol blue) supplemented with 5% β-mercaptoethanol. Samples were incubated at 55 °C for 25 min. 20 µL of each sample were loaded onto a polyacrylamide gel composed of a 10% resolving (lower) gel and a 6% stacking (upper) gel following staining with Coomassie blue staining and fractionated into eight fractions. Gel slices were cut into 1 mm³ cubes and destained with 50% acetonitrile (ACN) in 50 mM triethyl ammonium bicarbonate (TEAB) and dehydrated with pure CAN and dried in a vacuum concentrator. Sequencing grade modified trypsin (Promega) diluted by an ice-cold buffer containing 50 mM NH₄HCO₃ and 10% (v/v) ACN was added to cover the dehydrated gel pieces on ice. After 30 min, more trypsin-containing buffer was added to cover the expanded gel pieces followed by overnight incubation at 37 °C. Finally, the resulting tryptic peptides were extracted from the gel by equilibrating the samples with 50% ACN and 5% formic acid (FA) for 20 min in a 37 °C shaker. The extraction was repeated once, and all fractions were combined and vacuum dried. The protein digest was resuspended in 100 µl of 100 mM TEAB, and then 4 µl of 0.6 M sodium cyanoborohydride (NaBH₃CN) were added. Peptides from PI+ and Pi- were labeled with 4 µl of 4% formaldehyde (CH₂O) and deuterated formaldehyde (CD₂O), respectively. The reaction mixture was vortexed and incubated at room temperature for 1 h. The reaction was quenched by sequential addition of 16 µl of 1% (v/v) ammonia solution and 8 µl of formic acid. Finally, light- and heavy-labeled peptides were mixed, and vacuum dried immediately before further mass spectrometric analyses. Extracted peptides were analyzed by Nanoflow LC-MS/MS analyses using the EASY-nLC 1000 System (Thermo Scientific, USA) and LTQ Velos (Thermo Scientific, USA).

Data processing was performed following a previous description⁷⁰. For protein identification, MS/MS spectra were extracted from RAW files using MaxQuant (<http://maxquant.org/>, version 1.5.3.30). MASCOT (Matrix Science, version 2.3.02) was used to perform database search against an *E. coli* database (strain MG1655, with sequence files downloaded from UniProt in FASTA format, 4,358 entries. Average mass was selected with precursor mass tolerance of 1.5 Da and fragment mass tolerance of 0.8 Da. Methionine oxidation was set as a dynamic modification. The resulting assignments were filtered to achieve a false-discovery rate (FDR) of <1% at both the peptide and protein levels using the target-decoy method. Relative abundances of protein were represented by spectral counts, which are the number of repeated identification of peptides during the entire analysis.

To identify proteins that were differentially expressed in the sets of samples, the spectral counts data were subjected to statistic by DESeq package (Anders and Huber 2010) in R (Team 2014). Briefly, to eliminate the variance caused by sample loading and machine reading depth, the total counts data of two biological conditions was normalized to the same size. The following statistics were performed: *foldChange* (fold change from condition A to B), *pval* (p value for the statistical significance of this change), and *padj* (p value adjusted for multiple testing with the Benjamini-Hochberg procedure, which controls false discovery rate). Data set with *padj* <0.05 were considered to be significant (Anders and Huber 2010), and corresponding proteins were listed in S1 Table.

Polymyxin challenging assay

Challenging *E. coli* cells with designated concentration of polymyxin B (Sigma, USA) were performed as described with modifications⁷¹. *E. coli* cells grown under designated conditions were harvested by centrifugation at 13000 rpm for 1 min. Cell pellets were re-suspended in MOPS medium to a final concentration of 10⁸ cells/ml. The cell culture was treated with polymyxin B

with designated concentration for 1-3 hours at 37 °C without agitation. Cell culture prior to and following polymyxin treatment was plated on LB plate, CFU was counted after 12-16 hours incubation at 37°C. Survival of polymyxin challenging was determined by the survival rate of *E. coli* cells after drug treatment. Results are presented as the mean of three biological replicates.

Phylogenetic analysis of EcoPmrB homologs

The PmrB sequences from *E. coli* K-12 MG1655 were used as a query against γ -proteobacteria via BLASTP searches in the UniProt database, with an E-threshold of 10 and the BLOSUM62 substitution matrix. The top 250 retrieved sequences were aligned using the MUSCLE algorithm implemented in MEGA12 software. A phylogenetic tree of EcoPmrB homologous was constructed using the Maximum Likelihood method, with branch support assessed via adaptive bootstrap analysis using 562 bootstrap replicates in MEGA12. The JTT model was applied as the evolutionary model for tree construction.

Statistical analysis

Statistical analysis was performed using GraphPad Prism. Group comparisons between two groups were performed using two-tailed Student's *t* test. Group comparisons between multiple groups were performed using one-way ANOVA or two-way ANOVA with post hoc tests.

Supporting information

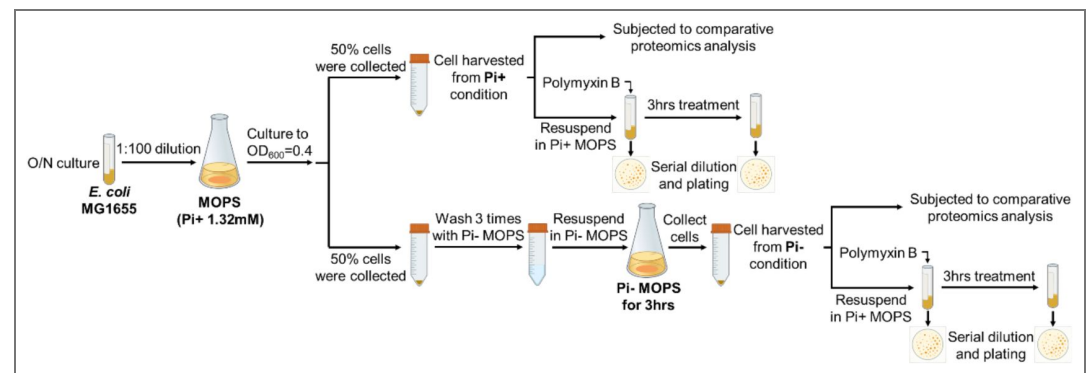


Figure S1. Workflow of acute Pi depletion treatment and following proteomic sample preparation and polymyxin B challenging assay. Bacteria were cultured to an OD_{600} of 0.4 in standard MOPS synthetic medium containing 1.32 mM inorganic phosphate (Pi), representing Pi-sufficient conditions. For Pi-depletion conditions, bacteria were first grown to $OD_{600} = 0.4$ in the same medium, then transferred to Pi-depleted MOPS medium (0 mM Pi). For comparative proteomic analysis, the collected bacterial cells were subjected to sample preparation and proteomic analysis. For the polymyxin challenging assay, the collected bacterial cells were resuspended in standard MOPS medium and treated with the designated concentration of polymyxin B. Cell viability was assessed at the beginning and end of treatment by serial dilution and plating.

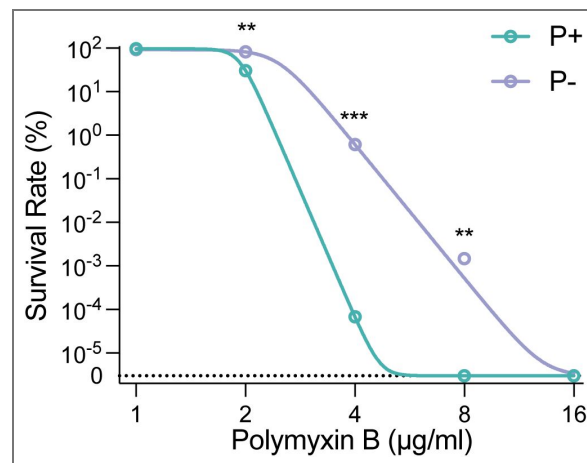


Figure S2. Killing of *E. coli* MG1655 with different concentration of polymyxin B.

Survival rates for *E. coli* MG1655 cells exposed 1-hour to polymyxin B (1-16 µg/ml) following acute Pi-starvation treatment (Pi-, 0 mM) compared to the group without treatment (Pi+, 1.32 mM). Error bars represent the standard deviation of at least three independent experiments. Statistical significance was determined using unpaired two-tailed Student's t-test. Significance levels are indicated as follows: * $p < 0.05$; ** $p < 0.01$; *** $p < 0.001$.

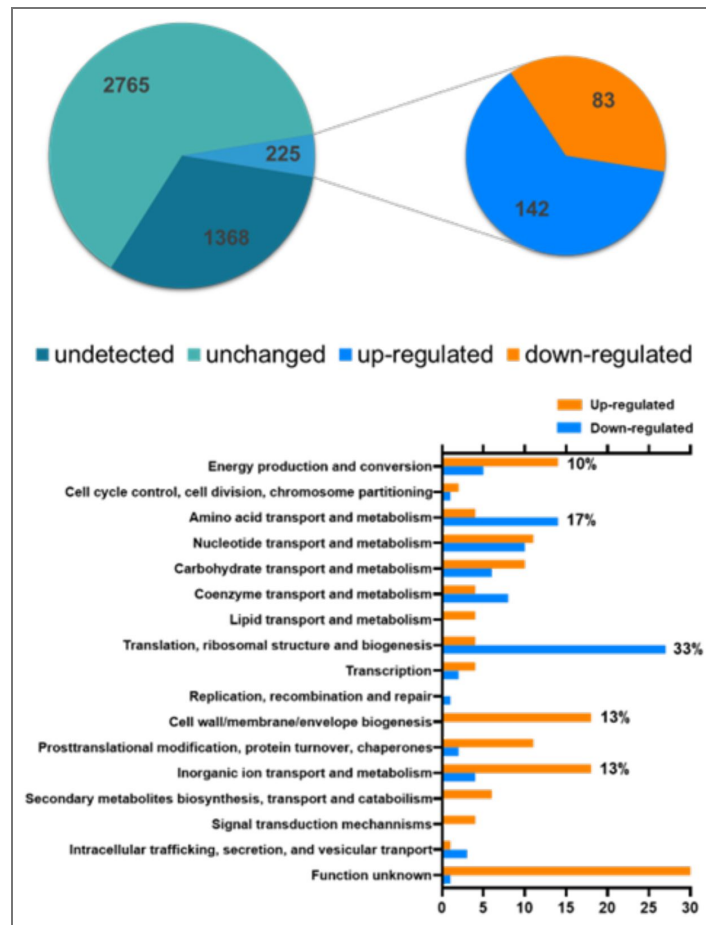


Figure S3. Quantitative proteomic analysis of *E. coli* MG1655 in response to acute Pi depletion.

Pie chart of total and differentially expressed proteins detected by LC-MS/MS analysis in *E. coli* MG1655 cells subjected to Pi depletion for 3 hours, relative to cells under Pi sufficient conditions. Red and blue colors represent significantly upregulated and downregulated proteins, respectively. Clusters of Orthologous Groups (COG) functional categories of differentially expressed proteins in *E. coli* MG1655 in response to Pi depletion. Red and blue colors represent significantly upregulated and downregulated proteins, respectively.

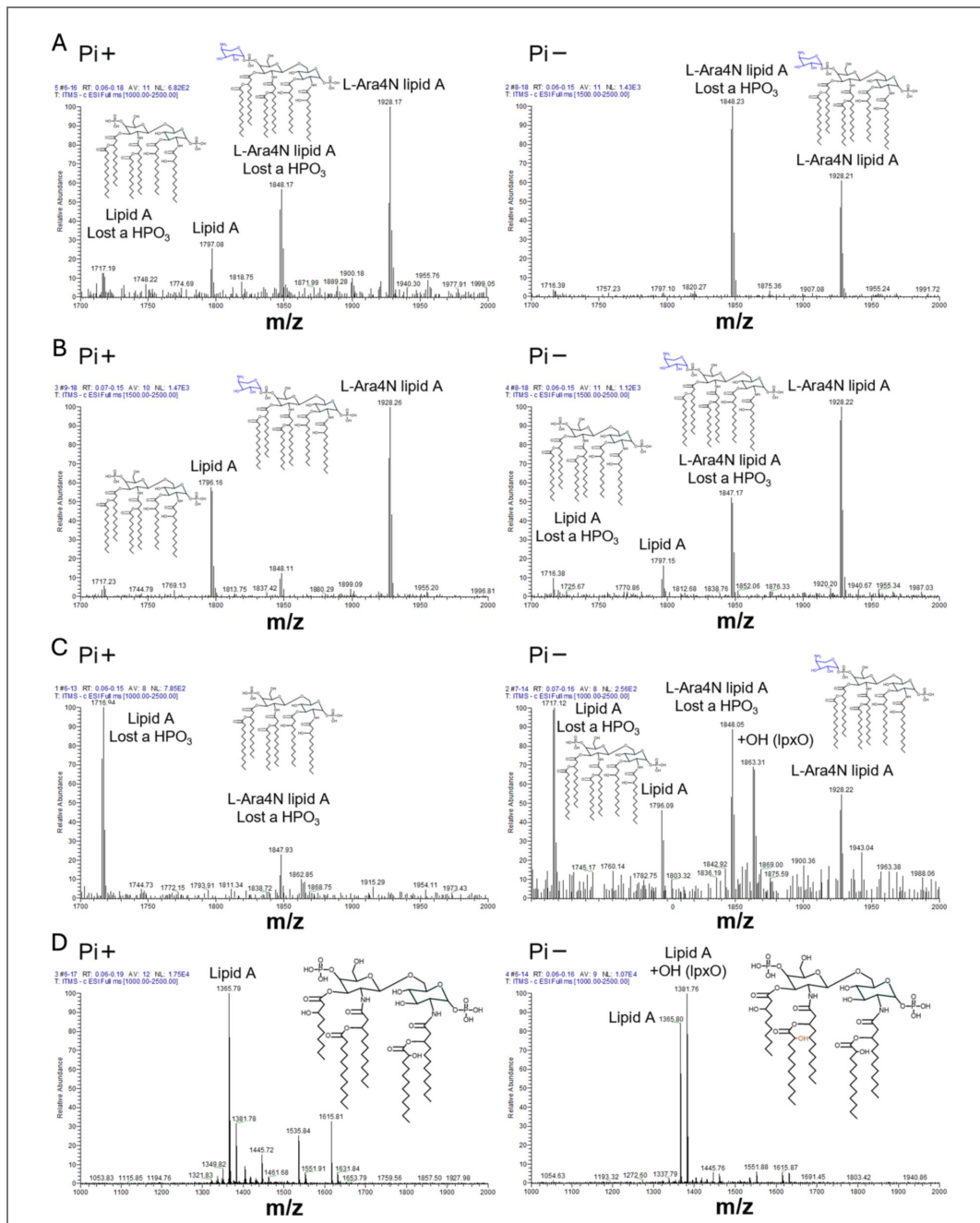


Figure S4. The ratio of L-Ara-4N modified Lipid A molecule increases in *E. coli* O157, *E. coli* UTI-3, *S. Typhimurium* ATCC14028 and *P. aeruginosa* PAO1 cells subjected to Pi depletion.

(A) ESI-MS spectra of lipid A molecules extracted from *E. coli* O157 cells following acute Pi-starvation treatment (Pi-, 0 mM) (right) compared to the group without treatment (Pi+, 1.32 mM) (left). Peaks correspond to native lipid A lost a HPO₃ (1718), native lipid A (1798), L-Ara-4N modified lipid A lost a HPO₃ (1848) and L-Ara-4N modified lipid A (1928) are shown. (B) ESI-MS spectra of lipid A molecules extracted from *E. coli* UTI-3 cells following acute Pi-starvation treatment (Pi-, 0 mM) (right) compared to the group without treatment (Pi+, 1.32 mM) (left). Peaks correspond to native lipid A lost a HPO₃ (1718), native lipid A (1798), L-Ara-4N modified lipid A lost a HPO₃ (1848) and L-Ara-4N modified lipid A (1928) are shown. (C) ESI-MS spectra of lipid A molecules extracted from *S. Typhimurium* ATCC14028 cells following acute Pi-starvation treatment (Pi-, 0 mM) (right) compared to the group without treatment (Pi+, 1.32 mM) (left). Peaks correspond to native lipid A lost a HPO₃ (1718), native lipid A (1798), L-Ara-4N modified lipid A lost a HPO₃ (1848), L-Ara-4N and -OH modified lipid A lost a HPO₃ (1863) and L-Ara-4N modified lipid A (1928) are shown. (D) ESI-MS spectra of lipid A molecules extracted from PAO1 cells following acute Pi-starvation treatment (Pi-, 0 mM) (right) compared to the group without treatment (Pi+, 1.32 mM) (left). Peaks correspond to hydroxylated lipid A lost a HPO₃ (1366), di-hydroxylated lipid A lost a HPO₃ (1382) are shown.

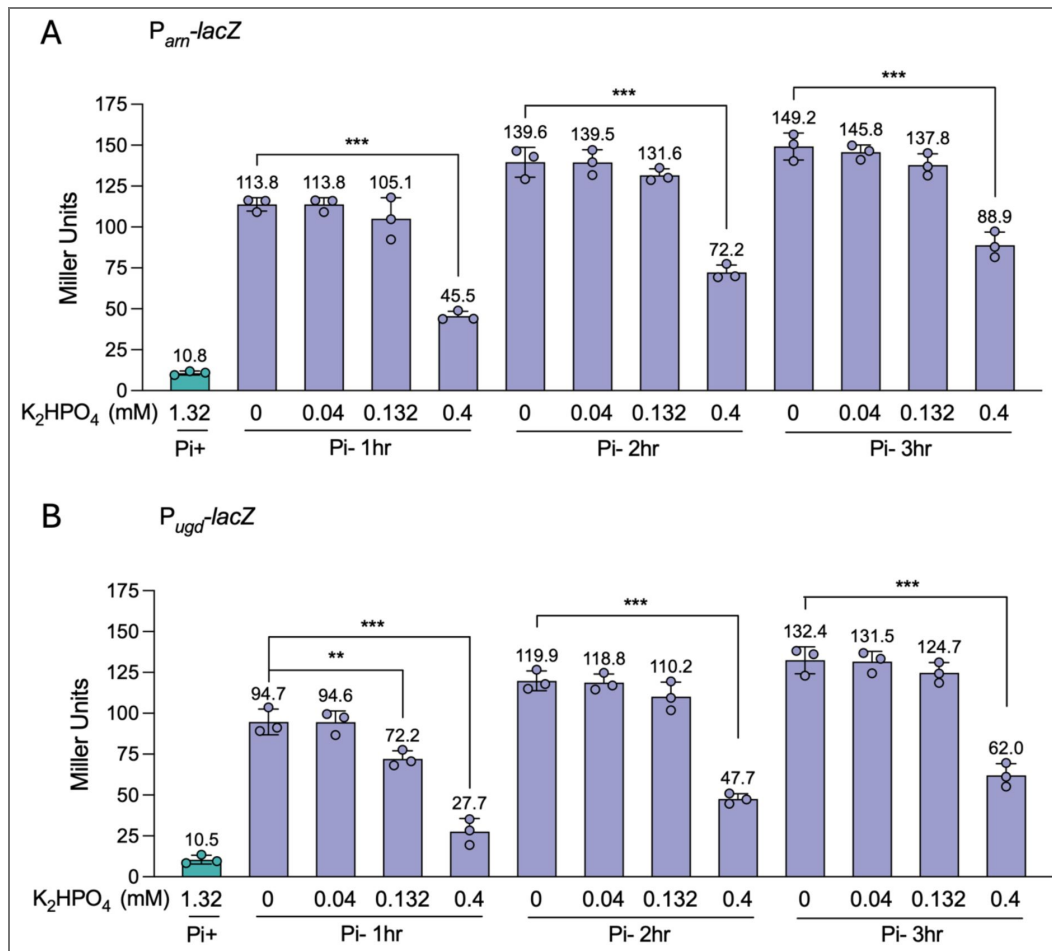


Figure S5. *Parn* and *Pugd* promoter activities in *E. coli* MG1655 during Pi depletion supplemented with different concentration of Pi.

(A) β -galactosidase activities of P_{arn} -*lacZ* in MG1655 Δ *lacZ* cells following Pi-starvation treatment with different concentration of Pi (Pi-, 0-0.4 mM) compared to the group without treatment (Pi+, 1.32 mM). (B) β -galactosidase activities of P_{ugd} -*lacZ* in MG1655 Δ *lacZ* cells following Pi-starvation treatment with different concentration of Pi (Pi-, 0-0.4 mM) compared to the group without treatment (Pi+, 1.32 mM). Error bars represent the standard deviation of at least three independent experiments. Statistical significance was determined using one-way ANOVA followed by Dunnett's multiple comparisons test. Significance levels are indicated as follows: * $p < 0.05$; ** $p < 0.01$; *** $p < 0.001$.

Figure S6. Up-regulation of *arn* genes during Pi depletion is independent of PhoBR and PhoPQ TCS in *E. coli* MG1655.

β -galactosidase activities of P_{ugd} -*lacZ* in MG1655 Δ *lacZ* parent and isogenic Δ *pmrB*, Δ *pmrA*, Δ *phoB* and Δ *phoR* mutants following acute Pi-starvation treatment (Pi-, 0 mM) compared to the group without treatment (Pi+, 1.32 mM). Error bars represent the standard deviation of at least three independent experiments. Statistical significance was determined using one-way ANOVA followed by Dunnett's multiple comparisons test. Significance levels are indicated as follows: * $p < 0.05$; ** $p < 0.01$; *** $p < 0.001$.

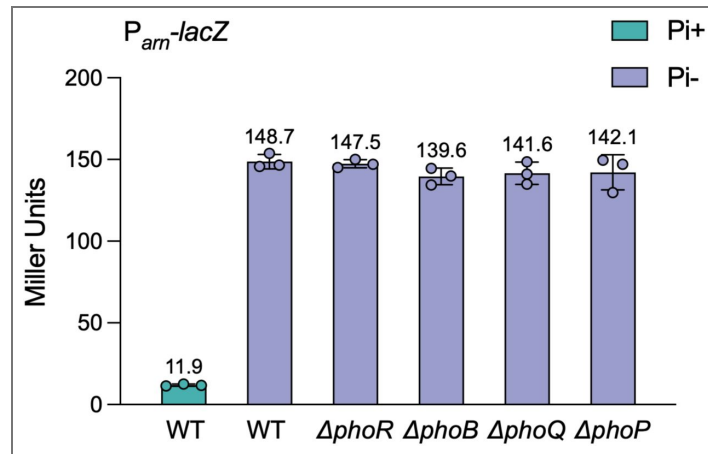


Figure S7. Up-regulation of *ugd* gene during Pi depletion is independent of PmrAB and PhoPQ TCS, but partially dependent on PhoBR TCS in *E. coli* MG1655.

β -galactosidase activities of P_{arn} -*lacZ* in MG1655 Δ *lacZ* parent and isogenic Δ *phoR*, Δ *phoB*, Δ *phoP* and Δ *phoQ* mutants following acute Pi-starvation treatment (Pi-, 0 mM) compared to the group without treatment (Pi+, 1.32 mM). Error bars represent the standard deviation of at least three independent experiments. Statistical significance was determined using one-way ANOVA followed by Dunnett's multiple comparisons test. Significance levels are indicated as follows: * $p < 0.05$; ** $p < 0.01$; *** $p < 0.001$.

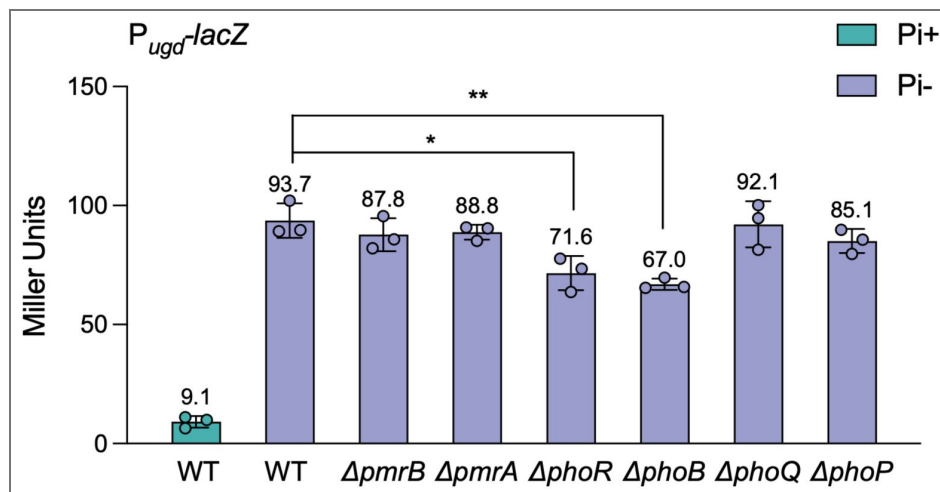


Figure S8. Pi depletion induced polymyxin tolerance is not affected in *eptA* deletion strain.

Survival of *E. coli* MG1655 parent and isogenic $\Delta eptA$ mutant exposed 1-hour to polymyxin B (4 $\mu\text{g}/\text{ml}$) following acute Pi-starvation treatment (Pi-, 0 mM) compared to the group without treatment (Pi+, 1.32 mM). Error bars represent the standard deviation of at least three independent experiments. Statistical significance was determined using two-tailed Student's t-test. Significance levels are indicated as follows: * $p < 0.05$; ** $p < 0.01$; *** $p < 0.001$.

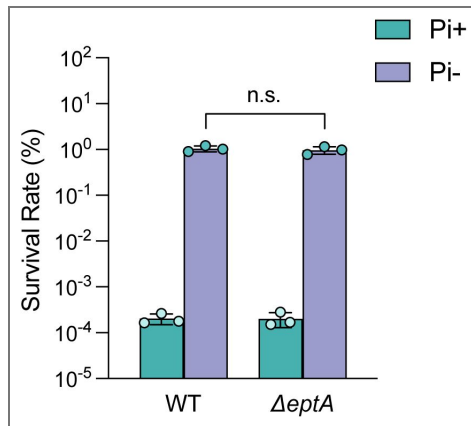


Figure S9. pH of spent medium of *E. coli* MG1655 after 5hrs Pi sufficient growth and after 3hrs Pi depletion treatment.

pH of the medium before bacteria inoculating and pH of the spent medium after 5hrs Pi sufficient growth or 3hrs Pi depletion treatment were measured. Error bars represent the standard deviation of at least three independent experiments.

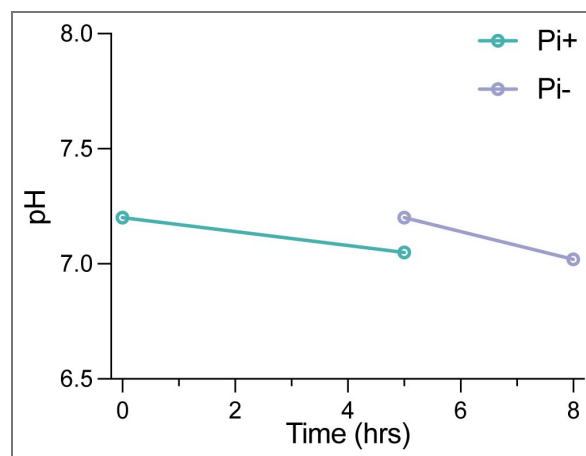


Figure S10. E36A and E39A mutation abolish the Fe³⁺ signaling capacity of PmrA.

β -galactosidase activities of $P_{amr}-lacZ$ in MG1655 $\Delta lacZ$ parent and isogenic $pmrB^{E36A}$, $pmrB^{E39A}$ mutants growth under MOPS minimal medium supplemented with different concentration of $FeSO_4$. Error bars represent the standard deviation of at least three independent experiments. Statistical significance was determined using two-way ANOVA followed by Dunnett's multiple comparisons test. Significance levels are indicated as follows: * $p < 0.05$; ** $p < 0.01$; *** $p < 0.001$.

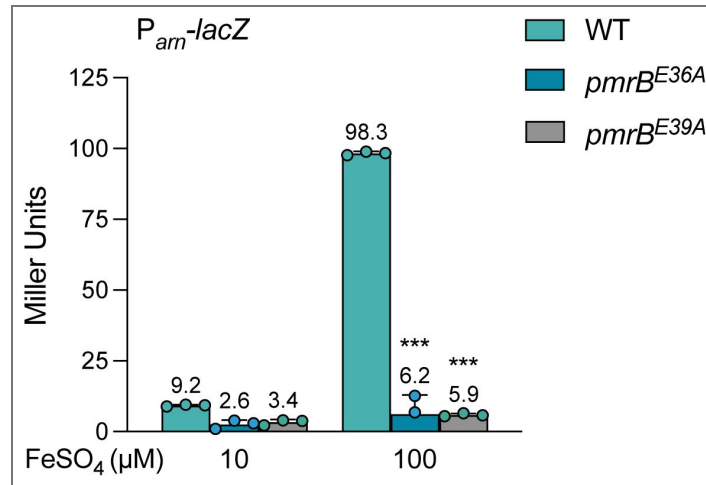


Figure S11. Deletion of canonical Fe³⁺ up-take genes does not affect the activation of PmrAB system and increase of Fe mobilization to *E. coli* cell during Pi depletion.

(A) β -galactosidase activities of $P_{amr}-lacZ$ in MG1655 $\Delta lacZ$ parent and isogenic $\Delta fecA$, $\Delta fepA$, $\Delta dentE$, Δfju , $\Delta cirA$, and $\Delta 5Fe$ ($\Delta fecA \Delta fepA \Delta dentE \Delta fju \Delta cirA$) mutants following acute Pi-starvation treatment (Pi-, 0 mM) compared to the group without treatment (Pi+, 1.32 mM). (B) Fe contents in *E. coli* MG1655 parent and isogenic $\Delta fecA \Delta fepA \Delta dentE \Delta fju \Delta cirA$ mutant following acute Pi-starvation treatment (Pi-, 0 mM) compared to the group without treatment (Pi+, 1.32 mM). Error bars represent the standard deviation of at least three independent experiments. Statistical significance was determined using one-way ANOVA followed by Dunnett's multiple comparisons test for A and two-way ANOVA followed by Sidak's multiple comparisons test for B. Significance levels are indicated as follows: * $p < 0.05$; ** $p < 0.01$; *** $p < 0.001$.

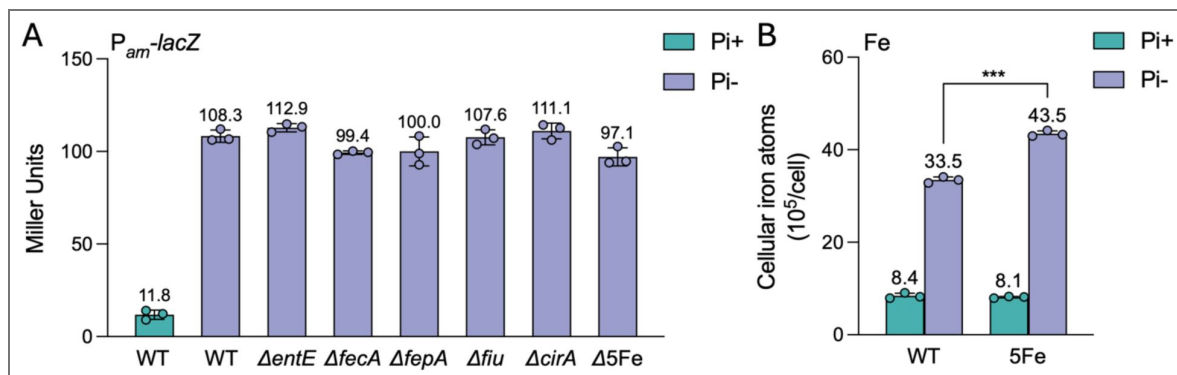


Figure S12. Decrease of cellular magnesium during Pi depletion is independent of Fe availability in medium.

Mg contents in *E. coli* MG1655 cell following Pi depletion treatment (0 Pi, 10 μM FeSO_4) or Fe-free Pi depletion treatment (0 Pi, 0 FeSO_4) at the indicated time points. Error bars represent the standard deviation of at least three independent experiments.

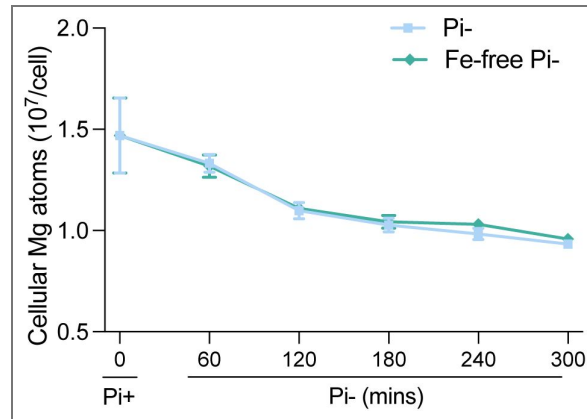
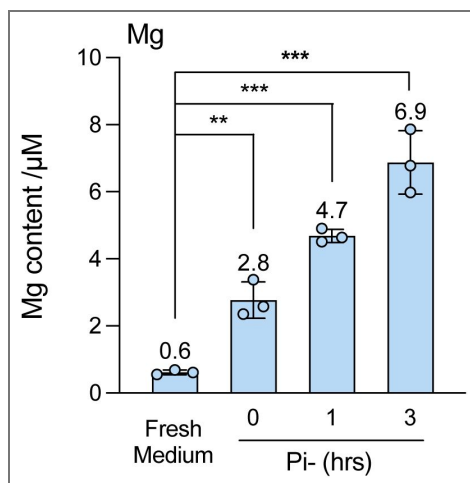


Figure S13. Magnesium disassociates from *E. coli* cells when subjected to Mg-free Pi-depleted medium.

Mg content in the spent medium during Mg-free Pi depletion treatment (0 Pi, 0 MgCl_2) at the indicated time points. Error bars represent the standard deviation of at least three independent experiments. Statistical significance was determined using one-way ANOVA followed by Dunnett's multiple comparisons test. Significance levels are indicated as follows: * $p < 0.05$; ** $p < 0.01$; *** $p < 0.001$.



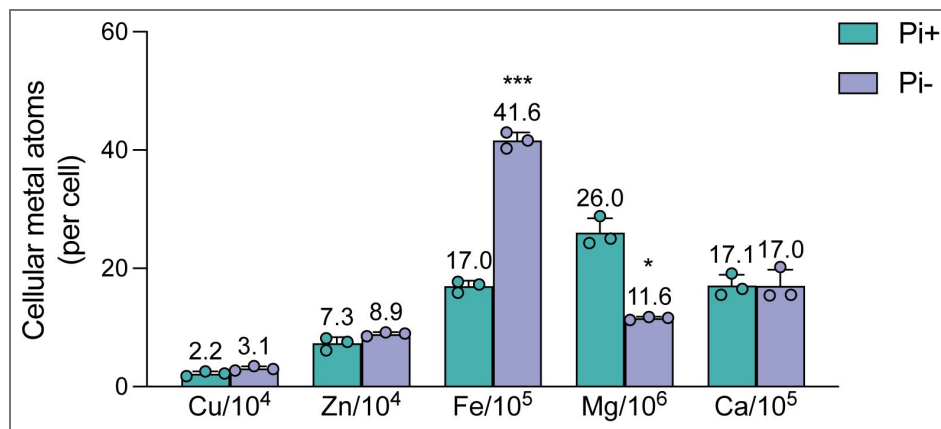


Figure S14. Cellular metal content in *P. aeruginosa* PAO1 cells with Pi depletion treatment and without Pi depletion treatment.

Cellular metal contents determined by ICP-MS in *P. aeruginosa* PAO1 cells following acute Pi-starvation treatment (Pi⁻, 0 mM) compared to the group without treatment (Pi⁺, 1.32 mM). Error bars represent the standard deviation of at least three independent experiments. Statistical significance was determined using two-tailed Student's t-test. Significance levels are indicated as follows: * $p < 0.05$; ** $p < 0.01$; *** $p < 0.001$.

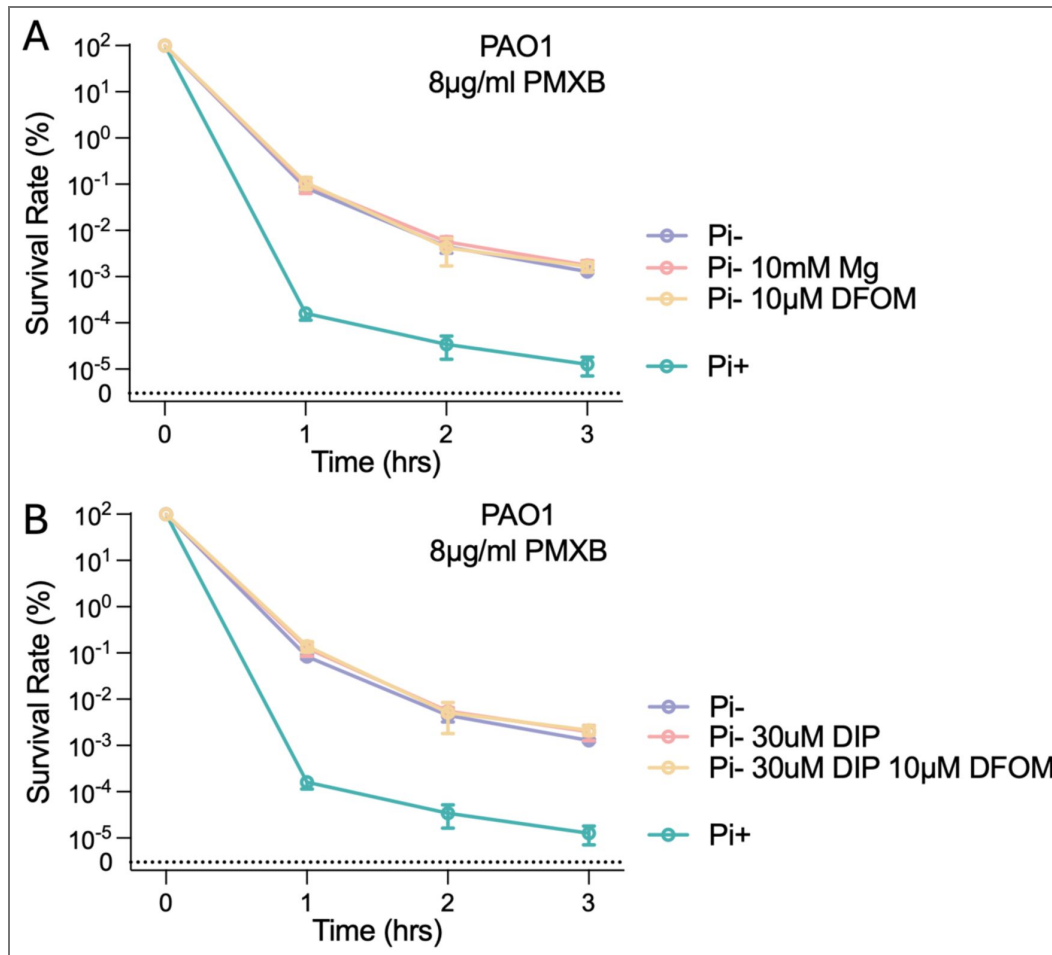


Figure S15. Disruption of Mg and Fe signaling showed no effect on Pi depletion induced polymyxin resistance in *P. aeruginosa*.

(A) Time-kill curves of *P. aeruginosa* PAO1 exposed to PMXB (8 µg/ml) following acute Pi-starvation treatment (Pi-, 0 mM Pi), Pi depletion treatment with excess Mg (Pi-, 0 mM Pi, 10mM MgCl₂) or Pi depletion treatment with iron chelator (Pi-, 0 mM Pi, 10 µM DFOM) compared to the group without treatment (Pi+, 1.32 mM Pi). (B) Time-kill curves of *P. aeruginosa* PAO1 exposed to PMXB (8 µg/ml) following acute Pi-starvation treatment (Pi-, 0 mM Pi), Pi depletion treatment with Fe²⁺ chelator (Pi-, 0 mM Pi, 30 µM DIP) or Pi depletion treatment with both Fe²⁺ and Fe³⁺ chelator (Pi-, 0 mM Pi, 30 µM DIP, 10 µM DFOM) compared to the group without treatment (Pi+, 1.32 mM Pi). Error bars represent the standard deviation of at least three independent experiments. Statistical significance was determined using one-way ANOVA followed by Dunnett's multiple comparisons test. Significance levels are indicated as follows: **p* < 0.05; ***p* < 0.01; ****p* < 0.001.

Figure S16. Cellular ATP level in *E. coli* MG1655 cells continuously decrease during Pi depletion.

Cellular ATP levels in *E. coli* MG1655 cells following Pi depletion treatment at the specified time points. Error bars represent the standard deviation of at least three independent experiments.

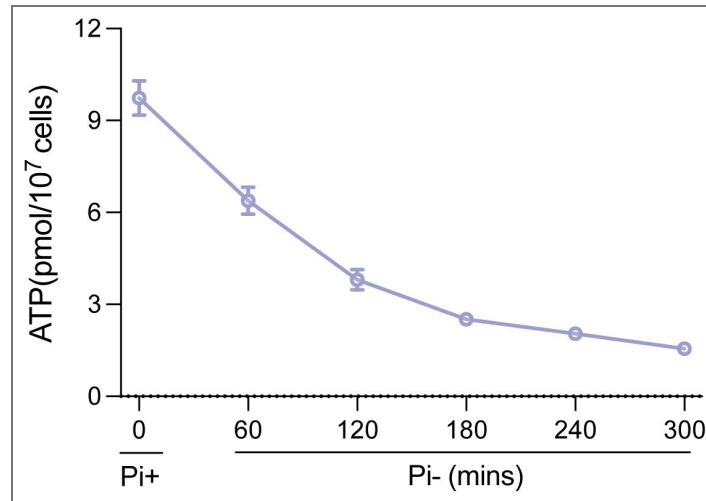


Figure S17. Lack of upregulation of *PphoQ* and *PmgtA* promoter activities indicates that the PhoPQ TCS is not activated during Pi depletion in *E. coli* MG1655.

β -galactosidase activities of *P_{phoQ}-lacZ* and *P_{mgtA}-lacZ* in MG1655 Δ *lacZ* parent following acute Pi-starvation treatment (Pi-, 0 mM) compared to the group without treatment (Pi+, 1.32 mM). Error bars represent the standard deviation of at least three independent experiments. Statistical significance was determined using two-tailed Student's t-test. Significance levels are indicated as follows: **p* < 0.05; ***p* < 0.01; ****p* < 0.001.

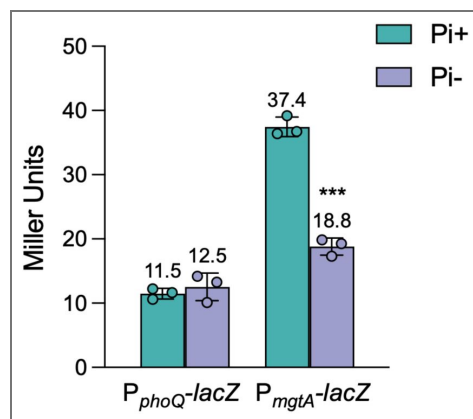


Figure S18. Up-regulation of both *P_{arn}* and *P_{ugd}* promoter activities during Pi depletion are not affected in *ppk* deletion strain.

(A) β -galactosidase activities of *P_{arn}-lacZ* in MG1655 Δ *lacZ* parent and isogenic *Δppk* mutant following acute Pi-starvation treatment (Pi⁻, 0 mM) compared to the group without treatment (Pi⁺, 1.32 mM). (B) β -galactosidase activities of *P_{ugd}-lacZ* in MG1655 Δ *lacZ* parent and isogenic *Δppk* mutant following acute Pi-starvation treatment (Pi⁻, 0 mM) compared to the group without treatment (Pi⁺, 1.32 mM). Error bars represent the standard deviation of at least three independent experiments. Statistical significance was determined using two-way ANOVA followed by Tukey's multiple comparisons test. Significance levels are indicated as follows: **p* < 0.05; ***p* < 0.01; ****p* < 0.001.

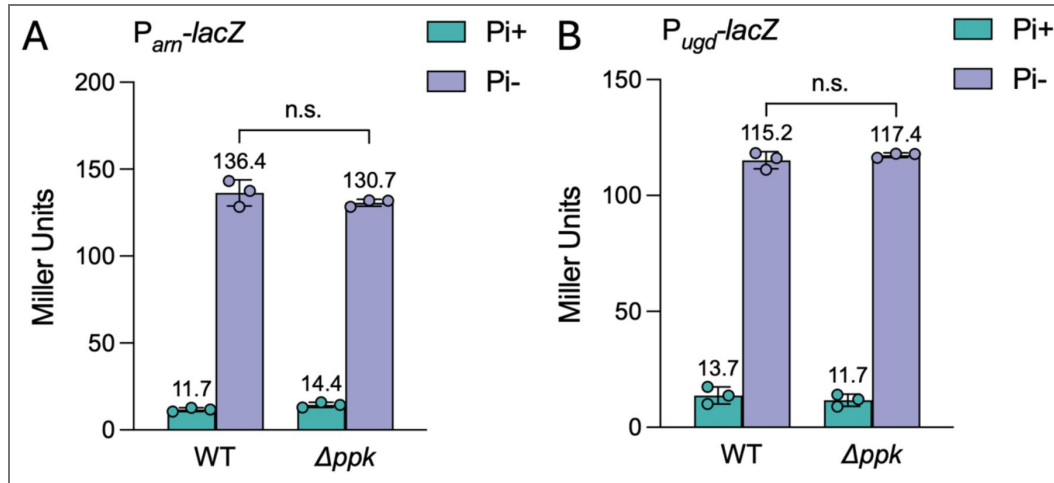
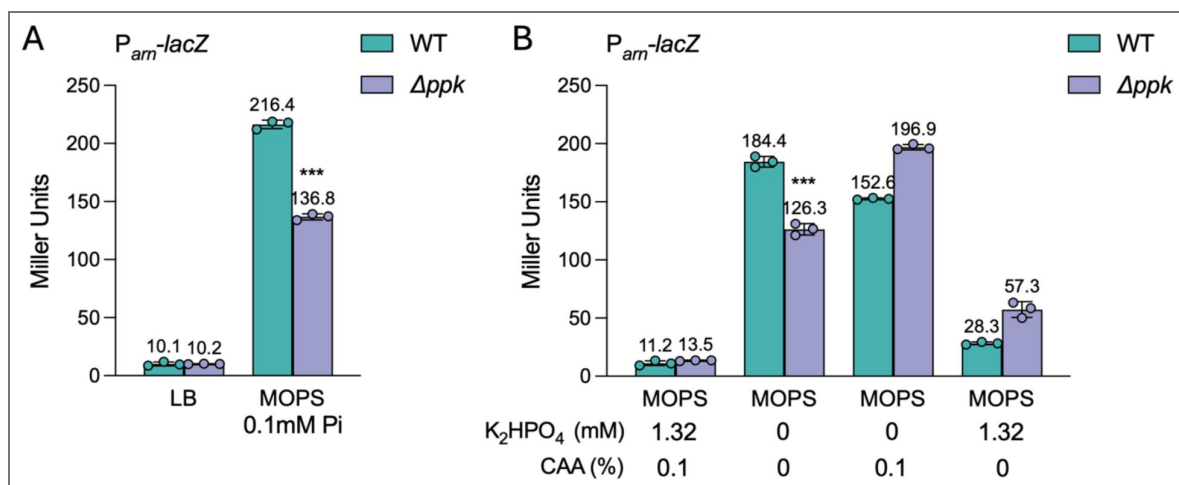


Figure S19. Pi depletion, amino acid depletion, and combined Pi-amino acid stress upregulate *P_{arn}* promoter activity, while *ppk* deletion only attenuates upregulation under combined stress.

(A) β -galactosidase activities of *P_{arn}-lacZ* in MG1655 Δ *lacZ* parent and isogenic *Δppk* mutant following acute nutrients downshift (MOPS 0.1 mM Pi) compared to the group without treatment (LB). Error bars represent the standard deviation of at least three independent experiments. Statistical significance was determined using two-way ANOVA followed by Tukey's multiple comparisons test. (B) β -galactosidase activities of *P_{arn}-lacZ* in MG1655 Δ *lacZ* parent and isogenic *Δppk* mutant following Pi depletion treatment (MOPS 0 Pi, 0.1% CAA), amino acid depletion treatment (MOPS 1.32 mM Pi, 0 CAA) and combined Pi-amino acid stress treatment (MOPS 0 Pi, 0 CAA) compared to the group without treatment (MOPS 1.32 mM Pi, 0.1% CAA). Error bars represent the standard deviation of at least three independent experiments. Statistical significance was determined using two-way ANOVA followed by Tukey's multiple comparisons test. Significance levels are indicated as follows: **p* < 0.05; ***p* < 0.01; ****p* < 0.001.



Strain	PMXB (ug/ml)
MG1655	0.5
O157	1
UTI-1	0.5
UTI-3	1
UTI-4	1
UTI-5	1
PAO1	0.5
ATCC 14028	2

Table S1. Minimum inhibitory concentrations (MICs) of strains in MOPS minimal medium

prot_desc	id	log2FoldChange	padj
argF	sp P06960 OTC2_ECOLI	-Inf	3.42E-18
gatZ	sp P0C8J8 GATZ_ECOLI	-Inf	3.77E-09
fis	sp P0A6R3 FIS_ECOLI	-Inf	2.78E-08
secY	sp P0AGA2 SECY_ECOLI	-Inf	0.000159211
kgtP	sp P0AEX3 KGTP_ECOLI	-Inf	0.001647533
gatC	sp P69831 PTKC_ECOLI	-Inf	0.002435201
cysC	sp P0A6J1 CYSC_ECOLI	-Inf	0.003341414
znuC	sp P0A9X1 ZNUC_ECOLI	-Inf	0.025826417
rffH	sp P61887 RMLA2_ECOLI	-Inf	0.036760697
cysD	sp P21156 CYSD_ECOLI	-5.525585778	1.38E-11
mnmG	sp P0A6U3 MNMG_ECOLI	-4.77187114	0.003253389
argA	sp P0A6C5 ARGA_ECOLI	-4.649638457	2.18E-06
yhjE	sp P37643 YHJE_ECOLI	-4.500028599	0.005992816
yegQ	sp P76403 YEGQ_ECOLI	-4.482584177	0.015352456
cysN	sp P23845 CYSN_ECOLI	-3.927062955	7.22E-14
pncB	sp P18133 PNCB_ECOLI	-3.639270989	6.73E-05
fbp	sp P0A993 F16PA_ECOLI	-3.600157407	0.023396164
moaA	sp P30745 MOAA_ECOLI	-3.529794204	0.018342621

Table S2. Proteins identified to be different expressed in *E. coli* MG1655 growing under Pi sufficient and depletion conditions

rpmC	sp P0A7M6 RL29_ECOLI	-3.142935813	1.68E-07
ilvN	sp P0ADF8 ILVN_ECOLI	-3.08821322	0.03765939
aroP	sp P15993 AROP_ECOLI	-2.833642328	0.021648588
deaD	sp P0A9P6 DEAD_ECOLI	-2.695068638	0.006647318
ilvB	sp P08142 ILVB_ECOLI	-2.690257592	1.41E-07
asnA	sp P00963 ASNA_ECOLI	-2.66746299	0.015909254
ptsG	sp P69786 PTGCB_ECOLI	-2.510708646	0.000188954
rpmD	sp P0AG51 RL30_ECOLI	-2.495454148	8.47E-09
ykgM	sp P0A7N1 RL31B_ECOLI	-2.483011177	0.00644327
gatB	sp P37188 PTKB_ECOLI	-2.418194429	0.035274735
cs	sp P0A972 CSPE_ECOLI	-2.352007644	4.54E-08
metA	sp P07623 META_ECOLI	-2.317452293	0.000139049
der	sp P0A6P5 DER_ECOLI	-2.267771633	0.0102137
potA	sp P69874 POTA_ECOLI	-2.183307337	0.03275735
leuA	sp P09151 LEU1_ECOLI	-1.998105409	1.07E-08
glf	sp P37747 GLF_ECOLI	-1.97691323	0.029751
tr	sp P00895 TRPE_ECOLI	-1.943830992	0.005678046
miaB	sp P0AEI1 MIAB_ECOLI	-1.92205685	0.004244044
pntB	sp P0AB67 PNTB_ECOLI	-1.852085802	9.85E-06
purF	sp P0AG16 PUR1_ECOLI	-1.826541229	4.76E-05
lepA	sp P60785 LEPA_ECOLI	-1.791966706	0.01657399

Table S2. (continued)

gatY	sp P0C8J6 GATY_ECOLI	-1.776699008	0.000182727
purT	sp P33221 PURT_ECOLI	-1.764435997	0.000643699
prfC	sp P0A7I4 RF3_ECOLI	-1.76312872	0.012506321
ybiC	sp P30178 YBIC_ECOLI	-1.727397747	0.01941163
rpsH	sp P0A7W7 RS8_ECOLI	-1.723379737	2.80E-10
purM	sp P08178 PUR5_ECOLI	-1.678278829	0.003764
cyoA	sp P0ABJ1 CYOA_ECOLI	-1.663437618	0.006838543
metL	sp P00562 AK2H_ECOLI	-1.661017127	0.00181135
leuC	sp P0A6A6 LEUC_ECOLI	-1.653771358	6.45E-06
pntA	sp P07001 PNTA_ECOLI	-1.595004247	7.61E-08
trxB	sp P0A9P4 TRXB_ECOLI	-1.571960722	0.002958769
metH	sp P13009 METH_ECOLI	-1.565084962	0.000869601
metC	sp P06721 METC_ECOLI	-1.510217214	0.025144896
rpmF	sp P0A7N4 RL32_ECOLI	-1.498744569	0.000469522
gyrA	sp P0AES4 GYRA_ECOLI	-1.448436432	7.72E-05
rpsR	sp P0A7T7 RS18_ECOLI	-1.418043759	3.03E-05
rpmG	sp P0A7N9 RL33_ECOLI	-1.381024188	0.006747605
purH	sp P15639 PUR9_ECOLI	-1.376402854	0.000114658
argI	sp P04391 OTC1_ECOLI	-1.37321011	0.000772873
rnb	sp P30850 RNB_ECOLI	-1.364231063	0.003951903
rplT	sp P0A7L3 RL20_ECOLI	-1.361561823	7.98781E-05

Table S2. (continued)

cysS	sp P21888 SYC_ECOLI	-1.352510933	0.018153582
metK	sp P0A817 METK_ECOLI	-1.28929395	0.000291382
sdhA	sp P0AC41 SDHA_ECOLI	-1.284366661	8.12E-05
ydjN	sp P77529 YDJN_ECOLI	-1.282130778	0.012801159
pyrD	sp P0A7E1 PYRD_ECOLI	-1.24642368	0.017272295
rpsM	sp P0A7S9 RS13_ECOLI	-1.231500265	4.82E-05
rpsC	sp P0A7V3 RS3_ECOLI	-1.228519333	5.14E-06
rplU	sp P0AG48 RL21_ECOLI	-1.200353979	0.000935979
pliG	sp P76002 PLIG_ECOLI	-1.192616084	0.023769411
rplB	sp P60422 RL2_ECOLI	-1.160209361	1.29E-05
rpsA	sp P0AG67 RS1_ECOLI	-1.154439475	2.19E-06
rplS	sp P0A7K6 RL19_ECOLI	-1.140490911	0.042048579
rpsT	sp P0A7U7 RS20_ECOLI	-1.136468494	0.000373058
thrA	sp P00561 AK1H_ECOLI	-1.131400346	7.55E-06
thrS	sp P0A8M3 SYT_ECOLI	-1.130800143	0.017957548
rplR	sp P0C018 RL18_ECOLI	-1.127973054	0.000234204
rplX	sp P60624 RL24_ECOLI	-1.108686244	0.000297915
aceB	sp P08997 MASY_ECOLI	-1.103226647	7.72E-05
aroA	sp P0A6D3 AROA_ECOLI	-1.074448834	0.048313271
rplI	sp P0A7R1 RL9_ECOLI	-1.074352178	3.31E-05
rplK	sp P0A7J7 RL11_ECOLI	-1.030031069	0.000940436

Table S2. (continued)

argH	sp P11447 ARLY_ECOLI	-1.029621386	0.010350803
cspC	sp P0A9Y6 CSPC_ECOLI	-1.010776163	0.00524746
gpmA	sp P62707 GPMA_ECOLI	1.007836346	0.000278112
gmhA	sp P63224 GMHA_ECOLI	1.02030343	0.027607596
luxS	sp P45578 LUXS_ECOLI	1.049588806	0.000506408
rpiA	sp P0A7Z0 RPIA_ECOLI	1.052561101	0.01318169
pgi	sp P0A6T1 G6PI_ECOLI	1.065800857	0.000188954
pykF	sp P0AD61 KPYK1_ECOLI	1.081019653	2.73E-05
mIaC	sp P0ADV7 MLAC_ECOLI	1.117643099	0.006345313
yfiF	sp P0AGJ5 YFIF_ECOLI	1.128896995	0.03275735
uspG	sp P39177 USPG_ECOLI	1.143746641	0.03765939
pgl	sp P52697 6PGL_ECOLI	1.167828441	0.01318169
deoC	sp P0A6L0 DEOC_ECOLI	1.174516518	0.018153582
grxB	sp P0AC59 GLRX2_ECOLI	1.178432467	0.000732045
fbaB	sp P0A991 ALF1_ECOLI	1.197658464	7.99E-05
adhE	sp P0A9Q7 ADHE_ECOLI	1.201151692	3.88E-07
degP	sp P0C0V0 DEGP_ECOLI	1.206061871	0.000278112
tas	sp P0A9T4 TAS_ECOLI	1.219282681	0.036014767
katG	sp P13029 KATG_ECOLI	1.220074858	7.01E-05
ribC	sp P0AFU8 RISA_ECOLI	1.272415628	0.030285161
pmbA	sp P0AFK0 PMBA_ECOLI	1.273270833	0.007784421

Table S2. (continued)

ftnA	sp P0A998 FTNA_ECOLI	1.301974436	0.010044367
moaB	sp P0AEZ9 MOAB_ECOLI	1.314241161	0.001746554
wrbA	sp P0A8G6 NQOR_ECOLI	1.34050881	4.33E-06
hdhA	sp P0AET8 HDHA_ECOLI	1.365397414	0.014224302
yahK	sp P75691 YAHK_ECOLI	1.380128931	0.000137547
acnA	sp P25516 ACNA_ECOLI	1.381383706	7.69E-05
sbp	sp P0AG78 SUBI_ECOLI	1.410886097	0.001647533
degQ	sp P39099 DEGQ_ECOLI	1.437968753	0.005431624
tktB	sp P33570 TKT2_ECOLI	1.45986506	7.28E-07
yjgA	sp P0A8X0 YJGA_ECOLI	1.470361111	0.0375636
glgP	sp P0AC86 PHSG_ECOLI	1.489480956	0.004703968
yggE	sp P0ADS6 YGGE_ECOLI	1.497996423	9.00E-05
mtlD	sp P09424 MTLD_ECOLI	1.508297143	0.007422869
cbpA	sp P36659 CBPA_ECOLI	1.520821408	0.040987772
deoB	sp P0A6K6 DEOB_ECOLI	1.533048098	8.38E-05
ybjP	sp P75818 YBJP_ECOLI	1.536131134	0.007427731
ybaY	sp P77717 YBAY_ECOLI	1.541925932	0.00084693
tdcE	sp P42632 TDCE_ECOLI	1.549713435	0.000108916
thiF	sp P30138 THIF_ECOLI	1.58507647	0.00235383
hdeB	sp P0AET2 HDEB_ECOLI	1.585194293	0.001902541
tpiA	sp P0A858 TPIS_ECOLI	1.585411082	9.28E-09

Table S2. (continued)

uspE	sp P0AAC0 USPE_ECOLI	1.605682754	0.000278112
rraA	sp P0A8R0 RRAA_ECOLI	1.607904489	0.000417551
yeaY	sp P0AA91 YEAY_ECOLI	1.609759679	0.001461256
nagD	sp P0AF24 NAGD_ECOLI	1.651426571	0.020565443
slp	sp P37194 SLP_ECOLI	1.661057589	0.000127411
osmC	sp P0C0L2 OSMC_ECOLI	1.671087683	3.90E-06
ycfP	sp P0A8E1 YCFP_ECOLI	1.676895218	0.000511934
acul	sp P26646 ACUI_ECOLI	1.680553338	0.001851227
pflB	sp P09373 PFLB_ECOLI	1.700478434	9.87E-14
lpoB	sp P0AB38 LPOB_ECOLI	1.721279546	0.000376072
clpB	sp P63284 CLPB_ECOLI	1.727347175	1.23E-12
gstB	sp P0ACA7 GSTB_ECOLI	1.748580068	0.001647533
slt	sp P0AGC3 SLT_ECOLI	1.751322485	0.015251337
yggN	sp P0ADS9 YGGN_ECOLI	1.768724665	0.049702565
loiP	sp P25894 LOIP_ECOLI	1.795763405	0.012616436
pspA	sp P0AFM6 PSPA_ECOLI	1.803047994	0.000834302
chrR	sp P0AGE6 CHRR_ECOLI	1.829520642	0.00084693
gstA	sp P0A9D2 GSTA_ECOLI	1.843282701	2.82E-06
msrA	sp P0A744 MSRA_ECOLI	1.871059945	0.023254637
dps	sp P0ABT2 DPS_ECOLI	1.8711205	1.92E-14
yghU	sp Q46845 YGHU_ECOLI	1.947282377	0.000291495

Table S2. (continued)

lldD	sp P33232 LLDD_ECOLI	1.949858867	0.035748827
yfcH	sp P77775 YFCH_ECOLI	1.988861376	0.015909254
cdd	sp P0ABF6 CDD_ECOLI	1.993269202	0.042932089
yeaG	sp P0ACY3 YEAG_ECOLI	2.011516734	4.21E-11
pqiB	sp P43671 PQIB_ECOLI	2.013507475	0.028681191
ygaU	sp P0ADE6 YGAU_ECOLI	2.059465726	3.23E-14
blc	sp P0A901 BLC_ECOLI	2.064974471	0.011100578
qorA	sp P28304 QOR1_ECOLI	2.155671369	4.33E-07
curA	sp P76113 CURA_ECOLI	2.175460559	0.010474873
bfr	sp P0ABD3 BFR_ECOLI	2.180562547	1.56E-13
yegP	sp P76402 YEGP_ECOLI	2.284730203	7.89E-10
ugd	sp P76373 UDG_ECOLI	2.340441236	0.018153582
yceF	sp P0A729 YCEF_ECOLI	2.382621181	0.040987772
yecA	sp P0AD05 YECA_ECOLI	2.405409463	0.03275735
bepA	sp P66948 BEPA_ECOLI	2.421711425	0.000774393
otsA	sp P31677 OTSA_ECOLI	2.448868257	6.65E-08
katE	sp P21179 CATE_ECOLI	2.50821371	2.35E-14
hchA	sp P31658 HCHA_ECOLI	2.50879706	2.75E-12
dkgA	sp Q46857 DKGA_ECOLI	2.649063918	1.64E-08
ybeL	sp P0AAT9 YBEL_ECOLI	2.658797186	3.16E-08
ymdB	sp P0A8D6 YMDB_ECOLI	2.671235984	0.024568779

Table S2. (continued)

fruB	sp P69811 PTFAH_ECOLI	2.672541661	1.42E-05
ydbC	sp P25906 YDBC_ECOLI	2.711914425	0.046758232
ynhG	sp P76193 YNHG_ECOLI	2.733690087	3.31E-05
yciE	sp P21363 YCIE_ECOLI	2.735728026	4.14E-05
ymbA	sp P0AB10 YMBA_ECOLI	2.798163878	0.036198317
ydcL	sp P64451 YDCL_ECOLI	2.82774542	2.04E-15
ldhA	sp P52643 LDHD_ECOLI	2.837647013	2.28E-05
amn	sp P0AE12 AMN_ECOLI	2.855927832	1.06E-13
yehZ	sp P33362 YEHZ_ECOLI	2.946432256	0.017149234
mdtE	sp P37636 MDTE_ECOLI	3.005567607	2.30E-05
gadB	sp P69910 DCEB_ECOLI	3.026824738	1.75E-33
yhjG	sp P37645 YHJG_ECOLI	3.114565954	0.004244044
gadC	sp P63235 GADC_ECOLI	3.122545884	0.000234696
gadA	sp P69908 DCEA_ECOLI	3.154673417	6.58E-36
ydhF	sp P76187 YDHF_ECOLI	3.156625723	5.19E-05
yjgR	sp P39342 YJGR_ECOLI	3.159652222	1.41E-12
yghA	sp P0AG84 YGHA_ECOLI	3.175685027	1.40E-09
ycaC	sp P21367 YCAC_ECOLI	3.185383669	2.44E-13
phoE	sp P02932 PHOE_ECOLI	3.204721908	2.80E-10
ycgM	sp P76004 YCGM_ECOLI	3.314835257	0.007920581
tam	sp P76145 TAM_ECOLI	3.330887068	0.010474873

Table S2. (continued)

yhbO	sp P45470 YHBO_ECOLI	3.335162899	0.000187361
phoR	sp P08400 PHOR_ECOLI	3.473374236	0.001325039
mdaB	sp P0AEY5 MDAB_ECOLI	3.504985139	1.26E-20
dkgB	sp P30863 DKGB_ECOLI	3.638374711	5.12E-09
yniA	sp P77739 YNIA_ECOLI	3.681925301	2.85E-07
gldA	sp P0A9S5 GLDA_ECOLI	3.74947351	3.13E-05
phnD	sp P16682 PHND_ECOLI	3.815420505	9.61E-10
ugpQ	sp P10908 UGPQ_ECOLI	4.003964005	1.04E-06
ahr	sp P27250 AHR_ECOLI	4.055942555	2.68E-05
pstS	sp P0AG82 PSTS_ECOLI	4.113208109	3.15E-56
cysQ	sp P22255 CYSQ_ECOLI	4.144617537	1.22E-07
glsA1	sp P77454 GLSA1_ECOLI	4.234450197	0.024320745
yciF	sp P21362 YCIF_ECOLI	4.316219533	0.000228764
ais	sp P45565 AIS_ECOLI	4.363027397	0.02438333
kefG	sp P0A756 KEFG_ECOLI	4.489497738	0.01318169
ydcS	sp P76108 YDCS_ECOLI	4.581943058	0.009304996
phnB	sp P16681 PHNB_ECOLI	4.606620186	4.21E-11
sodC	sp P0AGD1 SODC_ECOLI	4.625310091	1.37E-05
arnA	sp P77398 ARNA_ECOLI	4.698344251	1.36E-11
fic	sp P20605 FIC_ECOLI	4.74532692	0.001647533
ugpB	sp P0AG80 UGPB_ECOLI	4.789402823	1.62E-50

Table S2. (continued)

phoU	sp P0A9K7 PHOU_ECOLI	4.829226009	7.34E-29
kdpC	sp P03961 KDPC_ECOLI	4.927327983	0.001190624
pstB	sp P0AAH0 PSTB_ECOLI	5.294764534	6.41E-25
yebE	sp P33218 YEBE_ECOLI	5.774676565	1.18E-14
phoA	sp P00634 PPB_ECOLI	5.790096911	7.32E-85
phoB	sp P0AFJ5 PHOB_ECOLI	Inf	8.96E-35
arnB	sp P77690 ARNB_ECOLI	Inf	8.99E-08
appA	sp P07102 PPA_ECOLI	Inf	7.69E-05
yedP	sp P76329 MPGP_ECOLI	Inf	7.72E-05
ugpC	sp P10907 UGPC_ECOLI	Inf	0.000683993
arnC	sp P77757 ARNC_ECOLI	Inf	0.008862011
yfcG	sp P77526 YFCG_ECOLI	Inf	0.018153582
yraR	sp P45469 YRAR_ECOLI	Inf	0.012911411
yhhA	sp P0ADX7 YHHA_ECOLI	Inf	0.018724338
phnH	sp P16686 PHNH_ECOLI	Inf	0.025826417
gspJ	sp P45761 GSPJ_ECOLI	Inf	0.036463755
PmrA	sp P30843 PMRA_ECOLI	Inf	0.037433165
alpA	sp P33997 ALPA_ECOLI	Inf	0.037433165

Table S2. (continued)

Name	Description	Source
MG1655	<i>F</i> - λ - <i>ilvG</i> - <i>rfb</i> -50 <i>rph</i> -1 <i>E. coli</i> F^- <i>endA1</i> <i>glnV44</i> <i>thi</i> -1 <i>recA1</i> <i>relA1</i>	Lab collection
DH5 α	<i>gyrA96</i> <i>deoR</i> <i>nupG</i> <i>purB20</i> ϕ 80 <i>dlacZ</i> Δ M15 Δ (<i>lacZYA</i> - <i>argF</i>)U169, <i>hsdR17</i> ($r_K^- m_K^+$), λ^-	Lab collection
BI21 (DE3)	<i>E. coli</i> B F^- <i>ompT</i> <i>gal</i> <i>dcm</i> <i>lon</i> <i>hsdS_B</i> ($r_B^- m_B^-$) [<i>malB</i> ⁺] _{K-12} (λ^S)	Lab collection
<i>E. coli</i> O157	EHEC, O157:H7	Clinical isolate from Queen Mary Hospital (HK)
UTI-1	UPEC isolated from UTI patients	Clinical isolate from Queen Mary Hospital (HK)
UTI-3	UPEC isolated from UTI patients	Clinical isolate from Queen Mary Hospital (HK)
UTI-4	UPEC isolated from UTI patients	Clinical isolate from Queen Mary Hospital (HK)
UTI-5	UPEC isolated from UTI patients	Clinical isolate from Queen Mary Hospital (HK)
<i>Salmonella</i> ATCC14028	<i>Salmonella</i> ATCC14028 wild type	Lab collection
<i>P. aeruginosa</i>	<i>P. aeruginosa</i> PAO1 wild type	Lab collection

Table S3. Bacteria strains used in this study.

PAO1

AY7010	MG1655 ArnB-3xFLAG	This study
AY0416	MG1655 $\Delta lacZ::Km^R$	This study
AY4875	MG1655 $\Delta arnT:: Km^R$	This study
AY4860	MG1655 $\Delta arnB:: Km^R$	This study
AY4862	MG1655 $\Deltaugd:: Km^R$	This study
AY4858	MG1655 $\Delta pmrB:: Km^R$	This study
AY4859	MG1655 $\Delta pmrA:: Km^R$	This study
AY2741	MG1655 $\Delta phoB:: Km^R$	This study
AY2742	MG1655 $\Delta phoR:: Km^R$	This study
AY7011	MG1655 $\Delta pmrB:: Km^R \Delta lacZ$	This study
AY7012	MG1655 $\Delta pmrA:: Km^R \Delta lacZ$	This study
AY7013	MG1655 $\Delta phoB:: Km^R \Delta lacZ$	This study
AY7014	MG1655 $\Delta phoR:: Km^R \Delta lacZ$	This study
AY7015	MG1655 $\Delta lacZ, pmrB^{E36A}$	This study
AY7016	MG1655 $\Delta lacZ, pmrB^{E39A}$	This study
AY7017	MG1655 $\Delta pmrA$	This study
AY7018	MG1655 $pmrB^{E36A}$	This study
AY7019	MG1655 $pmrB^{E39A}$	This study
AY7020	MG1655 $\Delta fecA$	This study
AY7021	MG1655 $\Delta fecA$	This study

Table S3. (continued)

AY7022	MG1655 $\Delta entE$	This study
AY7023	MG1655 Δfiu	This study
AY7024	MG1655 $\Delta cirA$	This study
AY7025	MG1655 $\Delta fecA \Delta fepA \Delta entE \Delta fiu \Delta cirA$	This study

Table S3. (continued)

Name	Relevant characteristics	Source
pNN387	Single copy plasmid containing NotI and HindIII restriction sites before <i>lacZ</i>	Lab collection
pNN387(P _{<i>arn</i>} - <i>lacZ</i>)	Ligate promoter of <i>arn</i> into NotI/HindIII linearized pNN387	This study
pNN387(P _{<i>ugd</i>} - <i>lacZ</i>)	Ligate promoter of <i>ugd</i> into NotI/HindIII linearized pNN387	This study
pNN387(P _{<i>phoQ</i>} - <i>lacZ</i>)	Ligate promoter of <i>phoQ</i> into NotI/HindIII linearized pNN387	This study
pNN387(P _{<i>mgtA</i>} - <i>lacZ</i>)	Ligate promoter of <i>mgtA</i> into NotI/HindIII linearized pNN387	This study
pET28a-N	t7 promoter in pET-28a is replaced by araBad promoter	This study
pET28a-N-3xFLAG	C-terminal 6xHis tag in pET-28a-N is replaced by 3xFLAG tag	This study
pET-N-PmrA-6xHis	Ligate <i>pmrA</i> into NcoI/XhoI linearized pET-28a-N	This study
pET-N-PmrA-3xFLAG	Ligate <i>pmrA</i> into NcoI/XhoI linearized pET-28a-N-3xFLAG	This study
pET-N-PmrA137TAG-6xHis	Mutate G137 to TAG in pET28a-N-PmrA-6xHis	This study

Table S4. Plasmids used in this study.

pEVOL-CouA-RS	Plasmid expression CouA tRNA synthetase	Lab collection
pCAGO	Editing plasmid containing CRISPR-Cas9 and λ -red	Gift from Prof. Changhao Bi

Table S4. (continued)

Data availability

All data are available in the main text or the supplementary materials.

Acknowledgements

We thank Ms. Yining Chen in Prof. A. Yan's lab for proofreading the manuscript. We thank Prof. Changhao Bi (Tianjin Institute of Industrial Biotechnology, Chinese Academy of Sciences) for the generous gift of pCAGO plasmid. We thank Prof. Zhaochao Xu and Prof. Lu Miao (CAS Key Laboratory of Separation Science for Analytical Chemistry, Dalian Institute of Chemical Physics, Chinese Academy of Sciences) for the generous gift of OM-sensitive probe PI-BactD. We thank Prof. Patrick C. Y. Woo (Department of Microbiology, University of Hong Kong) for the generous gift of clinical *E. coli* strains.

Additional information

Funding

This work was supported by the

Research Grants Council of Hong Kong, Theme-based Research Scheme T21-705/20-N (A.Y. and T.Z.)

Natural Science Foundation of China 22193062 (T.Z.)

Research Grants Council of Hong Kong, Collaborative Research Fund C7033-20G (A.Y.)

National Key Research and Development Program of China 2022YFA1304500 (X.L.)

Natural Science Foundation of China 22174003 and 21974002 (X.L.)

Author contributions

Conceptualization: Guangming Zhang, Ziqing Deng, Aixin Yan.

Investigation Guangming Zhang, Ziqing Deng, Jiezhong Jiang, Minji Wang, Xiaoyuan Wang, Xiaoyun Liu, Aixin Yan.

Formal Analysis Guangming Zhang, Ziqing Deng, Xiaoyuan Wang, Xiaoyun Liu, Aixin Yan.

Funding Acquisition: Xiaoyun Liu, Aixin Yan.

Resources: Xiaoyuan Wang, Xiaoyun Liu, Aixin Yan.

Supervision: Xiaoyuan Wang, Xiaoyun Liu, Aixin Yan.

Visualization: Guangming Zhang.

Writing – original draft: Guangming Zhang, Aixin Yan.

Writing – review & editing: Guangming Zhang, Xiaoyun Liu, Aixin Yan.

Funding

Funder	Grant reference number	Author
Research Grants Council, University Grants Committee	T21-705/20-N	Aixin Yan
MOST National Natural Science Foundation of China (NSFC)	22193062	Aixin Yan
Research Grants Council, University Grants Committee	C7033-20G	Aixin Yan
MOST National Key Research and Development Program of China (NKPs)	2022YFA1304500	Xiaoyun Liu
MOST National Natural Science Foundation of China (NSFC)	22174003	Xiaoyun Liu

Author ORCID iDs

Aixin Yan:  <https://orcid.org/0000-0003-0310-5492>

References

1. Fang F.C., Frawley E.R., Tapscott T., Vázquez-Torres A (2016) Bacterial stress responses during host infection. *Cell host & microbe* **20**:133-143 <https://doi.org/10.1016/j.chom.2016.07.009> | PubMed
2. Poole K (2012) Bacterial stress responses as determinants of antimicrobial resistance. *Journal of Antimicrobial Chemotherapy* **67**:2069-2089 <https://doi.org/10.1093/jac/dks196> | PubMed
3. Wanner B.L (1996) Phosphorus assimilation and control of the phosphate regulon. In: Neidhardt F.C., Curtiss R.I., Gross C.A., Ingraham J.L., Lin E.C.C., Low K.B., Magasanik B., Reznikoff W., Schaechter M., Umberger H.E., et al. (Eds). *Escherichia coli and Salmonella: cellular and molecular biology* **1** pp. 1357-1381
4. Fagerbakke K.M., Heldal M., Norland S (1996) Content of carbon, nitrogen, oxygen, sulfur and phosphorus in native aquatic and cultured bacteria. *Aquatic Microbial Ecology* **10**:15-27 <https://doi.org/10.3354/ame010015>
5. Moore C., Mills M., Arrigo K., Berman-Frank I., Bopp L., Boyd P., Galbraith E., Geider R., Guieu C., Jaccard S (2013) Processes and patterns of oceanic nutrient limitation. *Nature geoscience* **6**:701-710 <https://doi.org/10.1038/ngeo1765>
6. Van Mooy B.A., Fredricks H.F., Pedler B.E., Dyhrman S.T., Karl D.M., Koblížek M., Lomas M.W., Mincer T.J., Moore L.R., Moutin T. (2009) Phytoplankton in the ocean use non-phosphorus lipids in response to phosphorus scarcity. *Nature* **458**:69-72 <https://doi.org/10.1038/nature07659> | PubMed
7. Vitousek P.M., Porder S., Houlton B.Z., Chadwick O.A (2010) Terrestrial phosphorus limitation: mechanisms, implications, and nitrogen-phosphorus interactions. *Ecological applications* **20**:5-15 <https://doi.org/10.1890/08-0127.1> | PubMed
8. George T.S., Hinsinger P., Turner B.L (2016) Phosphorus in soils and plants – facing phosphorus scarcity. *Plant and Soil* **401**:1-6 <https://doi.org/10.1007/s11104-016-2846-9>
9. Nguyen T.H., Wang B.X., Diaz O.R., Rajendram M., McKenna J.A., Butler D.S.C., Hokamp K., Hinton J.C.D., Monack D.M., Huang K.C (2025) Profiling Salmonella transcriptional dynamics during macrophage infection using a comprehensive reporter library. *Nature Microbiology* **10**:1006-1023 <https://doi.org/10.1038/s41564-025-01953-5> | PubMed
10. Röder J., Felgner P., Hensel M (2021) Single-cell analyses reveal phosphate availability as critical factor for nutrition of Salmonella enterica within mammalian host cells. *Cell Microbiol* **23**:e13374 <https://doi.org/10.1111/cmi.13374> | PubMed
11. Jones R.A., Shropshire H., Zhao C., Murphy A., Lidbury I., Wei T., Scanlan D.J., Chen Y (2021) Phosphorus stress induces the synthesis of novel glycolipids in *Pseudomonas aeruginosa* that confer protection against a last-resort antibiotic. *ISME J* **15**:3303-3314 <https://doi.org/10.1038/s41396-021-01008-7> | PubMed
12. Ferreira R.B.R., Antunes L.C.M., Sal-Man N (2025) Pathogen-pathogen interactions during co-infections. *Isme j* **19** <https://doi.org/10.1093/ismejo/wraf104> | PubMed
13. Murdoch C.C., Skaar E.P (2022) Nutritional immunity: the battle for nutrient metals at the host-pathogen interface. *Nature Reviews Microbiology* **20**:657-670 <https://doi.org/10.1038/s41579-022-00745-6> | PubMed
14. Rossi E., Falcone M., Molin S., Johansen H.K (2018) High-resolution in situ transcriptomics of *Pseudomonas aeruginosa* unveils genotype independent patho-phenotypes in cystic fibrosis lungs. *Nature Communications* **9** <https://doi.org/10.1038/s41467-018-05944-5> | PubMed

15. Sun N., Song Y., Liu C., Liu M., Yu L., Wang F (2021) Analysis of In Vivo Transcriptome of Intracellular Bacterial Pathogen *Salmonella enterica* serovar Typhmurium Isolated from Mouse Spleen. *Pathogens* **10** <https://doi.org/10.3390/pathogens10070823> | PubMed
16. Makino K., Shinagawa H., Amemura M., Kawamoto T., Yamada M., Nakata A (1989) Signal transduction in the phosphate regulon of *Escherichia coli* involves phosphotransfer between PhoR and PhoB proteins. *Journal of molecular biology* **210**:551-559 [https://doi.org/10.1016/0022-2836\(89\)90131-9](https://doi.org/10.1016/0022-2836(89)90131-9) | PubMed
17. Hsieh Y.-J., Wanner B.L (2010) Global regulation by the seven-component Pi signaling system. *Current opinion in microbiology* **13**:198-203 <https://doi.org/10.1016/j.mib.2010.01.014> | PubMed
18. Crépin S., Chekabab S.-M., Le Bihan G., Bertrand N., Dozois C.M., Harel J. (2011) The Pho regulon and the pathogenesis of *Escherichia coli*. *Veterinary microbiology* **153**:82-88 <https://doi.org/10.1016/j.vetmic.2011.05.043> | PubMed
19. Chekabab S.M., Harel J., Dozois C.M (2014) Interplay between genetic regulation of phosphate homeostasis and bacterial virulence. *Virulence* **5**:786-793 <https://doi.org/10.4161/viru.29307> | PubMed
20. Romano S., Schulz-Vogt H.N., González J.M., Bondarev V (2015) Phosphate limitation induces drastic physiological changes, virulence-related gene expression, and secondary metabolite production in *Pseudovibrio* sp. strain FO-BEG1. *Applied and environmental microbiology* **81**:3518-3528 <https://doi.org/10.1128/aem.04167-14> | PubMed
21. Pratt J.T., Ismail A.M., Camilli A (2010) PhoB regulates both environmental and virulence gene expression in *Vibrio cholerae*. *Molecular microbiology* **77**:1595-1605 <https://doi.org/10.1111/j.1365-2958.2010.07310.x> | PubMed
22. Jensen V., Löns D., Zaoui C., Bredenbruch F., Meissner A., Dieterich G., Münch R., Häussler S (2006) RhIR expression in *Pseudomonas aeruginosa* is modulated by the *Pseudomonas* quinolone signal via PhoB-dependent and-independent pathways. *Journal of bacteriology* **188**:8601-8606 <https://doi.org/10.1128/jb.01378-06> | PubMed
23. Ferreira G.M., Spira B (2008) The pst operon of enteropathogenic *Escherichia coli* enhances bacterial adherence to epithelial cells. *Microbiology* **154**:2025-2036 <https://doi.org/10.1099/mic.0.2008/016634-0> | PubMed
24. Romanowski K., Zaborin A., Fernandez H., Poroyko V., Valuckaite V., Gerdes S., Liu D.C., Zaborina O.Y., Alverdy J.C (2011) Prevention of siderophore-mediated gut-derived sepsis due to *P. aeruginosa* can be achieved without iron provision by maintaining local phosphate abundance: role of pH. *BMC microbiology* **11**:1-14 <https://doi.org/10.1186/1471-2180-11-212> | PubMed
25. Santos-Beneit F., Martin J.F (2013) Vancomycin resistance in *Streptomyces coelicolor* is phosphate-dependent but is not mediated by the PhoP regulator. *J Glob Antimicrob Resist* **1**:109-113 <https://doi.org/10.1016/j.jgar.2013.03.003> | PubMed
26. Dorrer E., Teuber M (1977) Induction of polymyxin resistance in *Pseudomonas fluorescens* by phosphate limitation. *Archives of Microbiology* **114**:87-89 <https://doi.org/10.1007/bf00429636> | PubMed
27. Olea-Ozuna R.J., Campbell M.J., Quintanilla S.Y., Nandy S., Brodbelt J.S., Boll J.M (2025) Alternative lipid synthesis in response to phosphate limitation promotes antibiotic tolerance in Gram-negative ESKAPE pathogens. *PLoS pathogens* **21**:e1012933 <https://doi.org/10.1371/journal.ppat.1012933> | PubMed
28. Lewenza S., Falsafi R., Bains M., Rohs P., Stupak J., Sprott G.D., Hancock R.E (2011) The *olsA* gene mediates the synthesis of an ornithine lipid in *Pseudomonas aeruginosa* during growth under phosphate-limiting conditions, but is not involved in antimicrobial peptide susceptibility. *FEMS Microbiol Lett* **320**:95-102 <https://doi.org/10.1111/j.1574-6968.2011.02295.x> | PubMed
29. Barbosa L.C., Goulart C.L., Avellar M.M., Bisch P.M., von Kruger W.M.A. (2018) Accumulation of ornithine lipids in *Vibrio cholerae* under phosphate deprivation is dependent on VC0489 (OlsF) and PhoBR system. *Microbiology* **164**:395-399 <https://doi.org/10.1099/mic.0.000607> | PubMed

30. Geiger O., Röhrs V., Weissenmayer B., Finan T.M., Thomas-Oates J.E (1999) The regulator gene *phoB* mediates phosphate stress-controlled synthesis of the membrane lipid diacylglyceryl-N,N,N-trimethylhomoserine in *Rhizobium* (*Sinorhizobium*) *melliloti*. *Mol Microbiol* **32**:63-73 <https://doi.org/10.1046/j.1365-2958.1999.01325.x> | PubMed
31. Lev S., Rupasinghe T., Desmarini D., Kaufman-Francis K., Sorrell T.C., Roessner U., Djordjevic J.T (2019) The PHO signaling pathway directs lipid remodeling in *Cryptococcus neoformans* via DGTS synthase to recycle phosphate during phosphate deficiency. *PLoS One* **14**:e0212651 <https://doi.org/10.1371/journal.pone.0212651> | PubMed
32. Geske T., Vom Dorp K., Dörmann P., Hölzl G. (2013) Accumulation of glycolipids and other non-phosphorous lipids in *Agrobacterium tumefaciens* grown under phosphate deprivation. *Glycobiology* **23**:69-80 <https://doi.org/10.1093/glycob/cws124> | PubMed
33. Gray R.M., Hunt D.M., Silva dos Santos M., Liu J., Agapova A., Rodgers A., Fearn A., Canseco J.O., Garza-Garcia A., MacRae J.I., *et al.* (2025) *Mycobacterium tuberculosis* overcomes phosphate starvation by extensively remodelling its lipidome with phosphorus-free lipids. *Nature Communications* **16** <https://doi.org/10.1038/s41467-025-66437-w> | PubMed
34. Vences-Guzman M.A., Geiger O., Sohlenkamp C (2012) Ornithine lipids and their structural modifications: from A to E and beyond. *FEMS microbiology letters* **335**:1-10 <https://doi.org/10.1111/j.1574-6968.2012.02623.x> | PubMed
35. Sohlenkamp C., Geiger O (2016) Bacterial membrane lipids: diversity in structures and pathways. *FEMS microbiology reviews* **40**:133-159 <https://doi.org/10.1093/femsre/fuv008> | PubMed
36. Kiriukhin M.Y., Debabov D.V., Shinabarger D.L., Neuhaus F.C (2001) Biosynthesis of the glycolipid anchor in lipoteichoic acid of *Staphylococcus aureus* RN4220: role of YpfP, the diglucosyldiacylglycerol synthase. *Journal of bacteriology* **183**:3506-3514 <https://doi.org/10.1128/jb.183.11.3506-3514.2001> | PubMed
37. Groat R.G., Schultz J., Zychlinsky E., Bockman A., Matin A (1986) Starvation proteins in *Escherichia coli*: kinetics of synthesis and role in starvation survival. *Journal of Bacteriology* **168**:486-493 <https://doi.org/10.1128/jb.168.2.486-493.1986> | PubMed
38. Raetz C.R., Reynolds C.M., Trent M.S., Bishop R.E (2007) Lipid A modification systems in gram-negative bacteria. *Annu. Rev. Biochem* **76**:295-329 <https://doi.org/10.1146/annurev.biochem.76.010307.145803> | PubMed
39. Ogasawara H., Shinohara S., Yamamoto K., Ishihama A (2012) Novel regulation targets of the metal-response BasS-BasR two-component system of *Escherichia coli*. *Microbiology* **158**:1482-1492 <https://doi.org/10.1099/mic.0.057745-0> | PubMed
40. Fernandez-Ciruelos B., Potmis T., Solomin V., Wells J.M (2023) Cross-talk between QseBC and PmrAB two-component systems is crucial for regulation of motility and colistin resistance in Enteropathogenic *Escherichia coli*. *PLoS Pathog* **19**:e1011345 <https://doi.org/10.1371/journal.ppat.1011345> | PubMed
41. Winfield M.D., Groisman E.A (2004) Phenotypic differences between *Salmonella* and *Escherichia coli* resulting from the disparate regulation of homologous genes. *Proceedings of the National Academy of Sciences* **101**:17162-17167 <https://doi.org/10.1073/pnas.0406038101> | PubMed
42. Wösten M.M., Kox L.F., Chamnongpol S., Soncini F.C., Groisman E.A (2000) A signal transduction system that responds to extracellular iron. *Cell* **103**:113-125 [https://doi.org/10.1016/s0092-8674\(00\)00092-1](https://doi.org/10.1016/s0092-8674(00)00092-1) | PubMed
43. Wang P., Zhang G., Xu Z., Chen Z., Liu X., Wang C., Zheng C., Wang J., Zhang H., Yan A (2022) Whole-cell FRET monitoring of transcription factor activities enables functional annotation of signal transduction systems in living bacteria. *J Biol Chem* **102258** <https://doi.org/10.1016/j.jbc.2022.102258> | PubMed
44. Wang J., Xie J., Schultz P.G (2006) A genetically encoded fluorescent amino acid. *Journal of the American Chemical Society* **128**:8738-8739 <https://doi.org/10.1021/ja062666k> | PubMed

45. **Chen H.D.**, Groisman E.A (2013) The biology of the PmrA/PmrB two-component system: the major regulator of lipopolysaccharide modifications. *Annual review of microbiology* **67**:83-112 <https://doi.org/10.1146/annurev-micro-092412-155751> | PubMed
46. **Lee L.J.**, Barrett J.A., Poole R.K (2005) Genome-wide transcriptional response of chemostat-cultured *Escherichia coli* to zinc. *Journal of bacteriology* **187**:1124-1134 <https://doi.org/10.1128/jb.187.3.1124-1134.2005> | PubMed
47. **Alves E.**, Moreirinha C., Faustino M.A., Cunha A., Delgadillo I., Neves M.G., Almeida A (2016) Overall biochemical changes in bacteria photosensitized with cationic porphyrins monitored by infrared spectroscopy. *Future Medicinal Chemistry* **8**:613-628 <https://doi.org/10.4155/fmc-2015-0008> | PubMed
48. **Breuer W.**, Epsztejn S., Cabantchik Z.I (1995) Iron Acquired from Transferrin by K562 Cells Is Delivered into a Cytoplasmic Pool of Chelatable Iron (II)(*). *Journal of Biological Chemistry* **270**:24209-24215 <https://doi.org/10.1074/jbc.270.41.24209> | PubMed
49. **Long S.**, Miao L., Li R., Deng F., Qiao Q., Liu X., Yan A., Xu Z (2019) Rapid Identification of Bacteria by Membrane-Responsive Aggregation of a Pyrene Derivative. *ACS Sens* **4**:281-285 <https://doi.org/10.1021/acssensors.8b01466> | PubMed
50. **Huang J.**, Li C., Song J., Velkov T., Wang L., Zhu Y., Li J (2020) Regulating polymyxin resistance in Gram-negative bacteria: roles of two-component systems PhoPQ and PmrAB. *Future microbiology* **15**:445-459 <https://doi.org/10.2217/fmb-2019-0322> | PubMed
51. **Hofstaedter C.E.**, Chandler C.E., Met C.M., Gillespie J.J., Harro J.M., Goodlett D.R., Rasko D.A., Ernst R.K (2024) Divergent *Pseudomonas aeruginosa* LpxO enzymes perform site-specific lipid A 2-hydroxylation. *Mbio* **15**:e02823-02823 <https://doi.org/10.1128/mbio.02823-23> | PubMed
52. **Pontes M.H.**, Sevostyanova A., Groisman E.A (2015) When too much ATP is bad for protein synthesis. *Journal of molecular biology* **427**:2586-2594 <https://doi.org/10.1016/j.jmb.2015.06.021> | PubMed
53. **Bruna R.E.**, Kendra C.G., Groisman E.A., Pontes M.H (2021) Limitation of phosphate assimilation maintains cytoplasmic magnesium homeostasis. *Proc Natl Acad Sci U S A* **118** <https://doi.org/10.1073/pnas.2021370118> | PubMed
54. **Klein D.J.**, Moore P.B., Steitz T.A (2004) The contribution of metal ions to the structural stability of the large ribosomal subunit. *Rna* **10**:1366-1379 <https://doi.org/10.1261/rna.7390804> | PubMed
55. **Pontes M.H.**, Groisman E.A (2018) Protein synthesis controls phosphate homeostasis. *Genes & development* **32**:79-92 <https://doi.org/10.1101/gad.309245.117> | PubMed
56. **Perez J.C.**, Shin D., Zwir I., Latifi T., Hadley T.J., Groisman E.A (2009) Evolution of a bacterial regulon controlling virulence and Mg²⁺ homeostasis. *PLoS genetics* **5**:e1000428 <https://doi.org/10.1371/journal.pgen.1000428> | PubMed
57. **Véscovi E.G.**, Soncini F.C., Groisman E.A (1996) Mg²⁺ as an extracellular signal: environmental regulation of *Salmonella* virulence. *Cell* **84**:165-174 [https://doi.org/10.1016/s0092-8674\(00\)81003-x](https://doi.org/10.1016/s0092-8674(00)81003-x) | PubMed
58. **Breazeale S.D.**, Ribeiro A.A., Raetz C.R (2002) Oxidative decarboxylation of UDP-glucuronic acid in extracts of polymyxin-resistant *Escherichia coli*: Origin of lipid a species modified with 4-amino-4-deoxy-l-arabinose. *Journal of Biological Chemistry* **277**:2886-2896 <https://doi.org/10.1074/jbc.m109377200> | PubMed
59. **Breazeale S.D.**, Ribeiro A.A., Raetz C.R (2003) Origin of Lipid A Species Modified with 4-Amino-4-deoxy-l-arabinose in Polymyxin-resistant Mutants of *Escherichia coli*: an aminotransferase (ArnB) that generates UDP-4-amino-4-deoxy-l-arabinose. *Journal of Biological Chemistry* **278**:24731-24739 <https://doi.org/10.1074/jbc.m304043200> | PubMed
60. **Yan A.**, Guan Z., Raetz C.R (2007) An undecaprenyl phosphate-aminoarabinose flippase required for polymyxin resistance in *Escherichia coli*. *J Biol Chem* **282**:36077-36089 <https://doi.org/10.1074/jbc.M706172200> | PubMed

61. Breazeale S.D., Ribeiro A.A., McClerren A.L., Raetz C.R (2005) A formyltransferase required for polymyxin resistance in *Escherichia coli* and the modification of lipid A with 4-amino-4-deoxy-l-arabinose: identification and function of UDP-4-deoxy-4-formamido-l-arabinose. *Journal of Biological Chemistry* **280**:14154-14167 <https://doi.org/10.1074/jbc.m414265200> | PubMed
62. Gunn J.S., Lim K.B., Krueger J., Kim K., Guo L., Hackett M., Miller S.I (1998) PmrA-PmrB-regulated genes necessary for 4-aminoarabinose lipid A modification and polymyxin resistance. *Molecular microbiology* **27**:1171-1182 <https://doi.org/10.1046/j.1365-2958.1998.00757.x> | PubMed
63. Stevenson G., Andrianopoulos K., Hobbs M., Reeves P.R (1996) Organization of the *Escherichia coli* K-12 gene cluster responsible for production of the extracellular polysaccharide colanic acid. *Journal of bacteriology* **178**:4885-4893 <https://doi.org/10.1128/jb.178.16.4885-4893.1996> | PubMed
64. Baijal K., Abramchuk I., Herrera C.M., Mah T.-F., Trent M.S., Lavallée-Adam M., Downey M (2024) Polyphosphate kinase regulates LPS structure and polymyxin resistance during starvation in *E. coli*. *Plos Biology* **22**:e3002558 <https://doi.org/10.1371/journal.pbio.3002558> | PubMed
65. Dahal P (2022) Enterobacteriaceae-definition, characteristics, identification. *Microbe Notes*.
66. Bligh E.G., Dyer W.J (1959) A rapid method of total lipid extraction and purification. *Canadian journal of biochemistry and physiology* **37**:911-917 <https://doi.org/10.1139/o59-099> | PubMed
67. Sahonero-Canavesi D.X., López-Lara I.M., Geiger O (2019) Membrane lipid degradation and lipid cycles in microbes. In: Rojo F (Ed). *Aerobic Utilization of Hydrocarbons, Oils, and Lipids* **10** pp. 978-973
68. Xu Z., Wang P., Wang H., Yu Z.H., Au-Yeung H.Y., Hirayama T., Sun H., Yan A (2019) Zinc excess increases cellular demand for iron and decreases tolerance to copper in *Escherichia coli*. *J Biol Chem* **294**:16978-16991 <https://doi.org/10.1074/jbc.RA119.010023> | PubMed
69. Zhao D., Feng X., Zhu X., Wu T., Zhang X., Bi C (2017) CRISPR/Cas9-assisted gRNA-free one-step genome editing with no sequence limitations and improved targeting efficiency. *Sci Rep* **7** <https://doi.org/10.1038/s41598-017-16998-8> | PubMed
70. Liu Y., Zhang Q., Hu M., Yu K., Fu J., Zhou F., Liu X (2015) Proteomic analyses of intracellular *Salmonella enterica* serovar Typhimurium reveal extensive bacterial adaptations to infected host epithelial cells. *Infection and immunity* **83**:2897-2906 <https://doi.org/10.1128/iai.02882-14> | PubMed
71. Groisman E.A., Kayser J., Soncini F.C (1997) Regulation of polymyxin resistance and adaptation to low-Mg²⁺ environments. *Journal of bacteriology* **179**:7040-7045 <https://doi.org/10.1128/jb.179.22.7040-7045.1997> | PubMed

Peer reviews

Reviewer #1 (Public review):

This manuscript by Zhang et al addresses how Pi scarcity/depletion drives PMB resistance in Enterobacteriaceae, because it proposes a mechanistically distinct pathway from the better-known PhoBR-linked phospholipid-remodeling responses in other Gram-negatives. The authors also suggest an intervention strategy based on Mg repletion or Fe chelation. The results are substantial and include genetic analyses, mass spectrometry, reporter assays, phospho-signaling readouts, metal quantification, and comparative analyses across enterobacterial species.

The paper reads well with the emphasis on the Mg loss followed by Fe mobilization during Pi depletion that induces PmrAB TCS activation for lipid A modification through transcriptional activation of *ugd* and *arn* genes. However, PmrAB is a well-known TCS responsible for PMB resistance through lipid A modification in the extensive studies by the Groisman lab. PmrA is a well-known transcriptional regulator to activate the transcription of the *ugd* gene in *Salmonella* and *Yersinia* by Mg depletion and Fe mobilization. Therefore, the current paper should focus more on the upstream signaling to connect the dots between Pi depletion and Mg loss. This is important because *Ugd* gene expression is not affected by PmrAB in Pi

depletion. It should also be considered that Mg loss is temporally associated with Fe mobilization, but the manuscript does not quantitatively show that Mg dissociation/redistribution is sufficient to trigger Fe mobilization in the absence of Pi depletion, considering that Mg is a macronutrient, whereas Fe is a micronutrient.

Second, the relationship between *arn* and *ugd* regulation needs a clearer mechanistic resolution to orchestrate the synthesis of the L-Ara4N during Pi depletion, because the manuscript shows that *arn* activation is PmrAB-dependent, whereas *ugd* is only partially PhoBR-dependent and not dependent on PmrAB. Yet the current model and narrative treat the system as a unified "*ugd-arn*" output. This should be carefully addressed, given that Pi depletion and Mg depletion might trigger different signaling modules.

Third, the manuscript argues that this is a "conserved" circuit in Enterobacteriaceae. The evidence for conservation is presently strongest in *E. coli* MG1655 and includes supportive observations in *E. coli* O157, one UTI strain by lipid A MS, several UTI isolates by killing assay, and *S. Typhimurium* for key phenotypes. No direct mechanistic validation is shown in other important genera belonging to Enterobacteriaceae, which include *Klebsiella*, *Enterobacter*, *Citrobacter*, *Yersinia*, *Serratia*, or other clinically important Enterobacteriaceae.

Fourth, the reversal and translational claims are a bit stronger than the current evidence supports. The title and Abstract state that identifying and targeting the circuit reverses Pi depletion-driven PMB, and the manuscript suggests a pharmacological intervention framework based on Mg supplementation or Fe chelation. The actual intervention evidence is limited to *in vitro* killing assays under acute Pi-depleted minimal-medium conditions in *E. coli* and *S. Typhimurium*, without *in vivo* testing, in that the experiments are performed under an acute 3-hour starvation in MOPS medium, not in host-mimicking or infection-relevant environments. The reversal needs to be shown not only at the level of survival curves, but also by the quantitative MIC/MBC measurements.

More importantly, the authors demonstrated that the signaling module upon Pi limitation in Enterobacteria differs from that in other Gram-negative bacteria such as Pseudomonads. However, they did not discuss why this difference would impact the life of Enterobacteria. The authors should consider the glycolytic pathways (i.e., EMP pathway for enterobacteria vs ED pathway for pseudomonads), in that the ED pathway requires less Pi, whereas the EMP pathway requires more Pi. It should be noted that Pi supply is highly limited in the natural environment for the free-living bacteria, rather than in the host environment for the commensals.

<https://doi.org/10.7554/eLife.111143.1.sa2>

Reviewer #2 (Public review):

Summary:

Using *E. coli* K-12 as a model system, the authors investigated how phosphate (Pi) depletion induces polymyxin resistance in Enterobacteriaceae, which notably lack the canonical phospholipid remodeling pathways commonly associated with phosphate starvation responses. They demonstrated that low-phosphate conditions promote L-Ara4N modification of lipid A, thereby enhancing polymyxin resistance. Proteomic analyses revealed significant upregulation of the *arn* operon and *ugd* under phosphate-limited conditions, and promoter activity assays further confirmed that both promoters are strongly induced during Pi depletion. Through gene deletion experiments, the authors showed that *arn* expression is regulated by the PmrAB two-component system, whereas *ugd* is controlled by PhoBR under low-phosphate conditions. Using ICP-MS analysis, they further found that phosphate limitation increases cell-associated Fe levels, and that reducing Fe availability abolishes PmrAB-dependent activation of the *arn* operon. Finally, the study demonstrated that Mg

supplementation and Fe chelation can suppress polymyxin resistance, highlighting the critical role of metal homeostasis in phosphate depletion-induced antimicrobial resistance.

Strengths:

Overall, I found this study to be well conducted, with convincing results that strongly support the proposed model. Through comprehensive genetic analyses and detailed characterization of metal ion homeostasis and membrane lipid modifications, the authors uncovered a novel regulatory connection among Mg^{2+} , Fe^{3+} , and the PmrAB pathway, a key driver of polymyxin resistance. These findings are highly interesting and have important implications for understanding the evolution of the Fe-sensing PmrAB system, as well as the broader role of nutrient availability in shaping antibiotic resistance.

Weaknesses:

I did not identify any particular weaknesses.

<https://doi.org/10.7554/eLife.111143.1.sa1>

Reviewer #3 (Public review):

Summary:

This manuscript examines how phosphate limitation primes *E. coli* and *Salmonella* for defense against polymyxin antibiotics. Other environmental signals, such as altered levels of extracellular Mg or Fe, were previously shown to induce polymyxin resistance in Enterobacteriaceae, and phosphate limitation was known to augment polymyxin resistance in other organisms such as *A. baumannii* and *P. aeruginosa*; however, whether phosphate limitation boosted polymyxin resistance in Enterobacteriaceae was not known. This study shows that this indeed occurs, and the mechanism is distinct from that in *A. baumannii* and *P. aeruginosa*. The model proposed is: (1) low phosphate causes bacteria to jettison Mg to balance cellular P/Mg ratio, (2) extracellular Fe^{3+} associates with the cell envelope to replace Mg as LPS-bridging cation, and (3) envelope Fe^{3+} activates PmrAB, which mediates a transcriptional response leading to L-Ara4N modification of lipid A and protection from polymyxin B. Flooding with Mg or chelating the surface Fe^{3+} blocks the protective response to low phosphate in *E. coli* and *Salmonella* but not in *P. aeruginosa* despite Fe still mobilizing in the latter. The differential response between Enterobacteriaceae and *P. aeruginosa* is connected to the presence/absence of Fe-sensing motifs in the PmrB periplasmic domain.

Strengths:

The strengths of the study are the wide array of approaches used and the thorough characterization of a novel stress-response mechanism involving metal mobilization. Combined with the analysis of multiple bacterial families, the results clarify how different strategies have evolved to defend against polymyxins during phosphate starvation.

Weaknesses:

Controls are needed in some of the genetic experiments, namely complementation, to verify linkage of defective survival phenotypes to the genes mutated and to rule out protein stability defects for the PmrB variants tested. In addition, the generalizability of the metal mobilization feature of the model would be strengthened by examining media with differing metal composition. Claims about antibiotic resistance would be strengthened by data examining bacterial growth in the presence of an antibiotic.

<https://doi.org/10.7554/eLife.111143.1.sa0>